Optical pulse compression of first anti-Stokes order in the multi-frequency Raman generation with the presence of red shifted shoulder

By

Abdullah Rahnama

A thesis
presented to the University of Waterloo
in fulfilment of the
thesis requirement for the degree of
Master of Science
in
Physics

Waterloo, Ontario, Canada, 2018

I hereby declare that I am the sole author of this thesis. This is a true copy of the thesis, including any required final revisions, as accepted by my examiners.

I understand that my thesis may be made electronically available to the public.

Abstract:

Multi-frequency Raman generation (MRG) is a nonlinear technique to generate intense trains of single-femtosecond pulses. The broad spectrum of different Raman orders which is spread from near-infrared (near-IR) to UV can be used to make single-femtosecond pulses. Albeit, this technique cannot compete with high harmonic generation technique (HHG) in pulse duration, the small frequency spacing between different Raman orders causes to increase the temporal spacing between the pulses, which will eventually increase the pulse power. MRG can be used in many different nonlinear optics applications, which need intense short laser pulses.

To generate short laser pulses, the phase of each Raman order should first be corrected; then, by coherently adding all the different orders, it is possible to get the shortest pulse. We have experimentally observed that the Raman orders can be broadened and have a shoulder in the lower frequency. In the best case, the first anti-stokes bandwidth can be doubled. This effect can cause fewer pulses in the final pulse train, thereby significantly increasing the power of each pulse.

In this thesis, we use a pulse compression system based on prism pairs to compress the first Raman order in the presence and absence of red-shifted shoulder.

We are also interested in how the temporal behavior of red-shifted shoulder and the Raman order will be changed by using our pulse compression system, and generally, how this red-shifting can be used in the generation of intense ultra-short laser pulses.

Acknowledgements

I want to thank my supervisor Dr. Donna Strickland for giving me the opportunity to work in her research lab and the help and guidance on my research project. I would also like to thank Dr. Joseph Sanderson, Dr. Donna Strickland, and Dr. James Martin for being on my defense committee. I also wish to thank Dr. Kostadinka Bizheva, and Dr. Amir Hamed Majedi for being on my Masters committee these last two years. I would also like to thank my fellow student Zujun Xu for his help and support during these two years. Finally, I would also like to acknowledge all my family and group members in the lab, Tuyen, Xinyang, Michael, and Ali for their friendships and supports.

Dedication

Dedicated to the precious memories of my father (the late Dr. Majid Rahnama) who was my biggest supporter in my life and in choosing physics as my major like himself, and to follow my dreams. Alas, no words can express my love, feelings, … for him. May God bless him.

Table of Contents

List of Figures

List of Tables

List of Abbreviations

BBO	ß-barium-borate
CCD	Charge-coupled device
CPA	Chirped pulse amplification
FWHM	Full width at half maximum
GDD	Group-delay dispersion
GVD	Group-velocity dispersion
HHG	High harmonic generation
IR	Infra red
KLM	Kerr lens mode-locking
MRG	Multi frequency Raman generation
OSA	Optical spectrum analyzer
SRS	Stimulated Raman scattering
SPM	Self phase modulation
SF_6	Sulfur hexafluoride
SF10	Dense flint glass
TOD	Third order dispersion
UV	Ultraviolet
XUV	Extreme ultraviolet

List of Physical Symbols

ϵ	Dielectric constant
ϵ_0	Vacuum permittivity
λ	Wavelength
μ	Vacuum permeability
n	Refractive index
f	Frequency
$\phi(\omega)$	Spectral phase
$\varphi(t)$	Temporal phase
χ	Susceptibility
χ^1	Linear dielectric susceptibility
χ^2	Second order nonlinear susceptibility
χ^3	Third order nonlinear susceptibility
χ^5	Fifth order nonlinear susceptibility
ω	Angular frequency
ω_0	Carrier angular frequency

"I do not know what I may appear to the world, but to myself I seem to have been only like a boy playing on the seashore, and diverting myself in now and then finding a smoother pebble or a prettier shell than ordinary, whilst the great ocean of truth lay all undiscovered before me."

Sir Isac Newton

Chapter 1

Introduction

"I have set my rainbow in the clouds, and it will be the sign of the covenant between me and the earth." [1]

More than 300 years has been passed from the day that Sir Isaac Newton showed that the covenant between the lord and the earth can be seen everywhere, only a dispersive material is needed to show us this beauty. Our research goal is to make high power single femtosecond pulses from the lord's rainbow.

Today's technology is based on the accuracy of our measurements. As we make more progress in many different areas, we need to have a better understanding of the superfast processes. Ultrafast optics provides us the tool to increase our temporal resolution. These days, ultra-short laser pulses have many different applications in different areas such as ultrafast spectroscopy, laser-controlled chemistry, frequency metrology, optical communication, materials processing, biomedical application, etc. These applications have one thing in common, and that is a short burst of light.

After the invention of lasers, many different methods have been invented to create short laser pulses. Q-switching, mode-locking, high order harmonic generation (HHG), and multi frequency Raman generation (MRG) are different methods to create short lasers pulses with different pulse duration and energy.

Today, Ti:sapphire oscillators can easily generate pulses as short as five femtoseconds [2], and HHG can generate the shortest pulses in attosecond regime [3], which can enable us to look at electrons in slow-motion [1]. In this chapter, we will review different techniques for generating short laser pulses, and finally explain the MRG's advantages for generation of short laser pulses.

1.1 Different Methods to Create Short Laser Pulses

1.1.1 Q-Switching

One of the first methods that have been used to create short laser pulses is Q-switching method. The word 'Q' comes from 'quality factor', which plays a crucial role in designing any laser resonator. Q factor in laser physics is related to the loss inside a resonator. Basically, the resonators with high Q-factors are highly desirable. To generate short laser pulses, we can suddenly change the Q factor of a laser cavity by an active or passive device. By changing the Q factor, we are changing the loss inside the resonator. So, how does this loss make a short laser pulse?

In a lasing CW laser, the gain is always higher than the loss. Atoms are pumped up continuously to higher states, and thereafter by having stimulated emission, they will come to a lower state. Then, we have steady output power. In the Q-switching, we create a temporary loss inside our system. This means that we stop atoms having the stimulated emission. The atoms will be pumped to the higher states, but they cannot come to the lower state because we have created the loss in the system. Suddenly the loss of the system will be changed, and all the atoms come to lower state. Finally, we have a powerful short pulse [4]. This is the basic mechanism of Q- switching. By creating the loss, or in other words, by changing the Q factor of the resonator, we can have a short laser pulse with high intensity. This changing of the loss inside the resonator can be done by putting active loss modulators (acousto optical modulators [5]or RF modulators) or passive modulators (saturable absorbers [6]) inside the cavity of a laser. The duration of output pulses will be a function of two factors. The first one is the lifetime of the atoms at higher state, which strongly depends on the laser gain medium. The second one is how fast we can change the loss of our system. Usually, the output pulse can have a pulse duration of a few micro seconds to tens of picoseconds with the energy of tens of mJ in each pulse [7]. In the Q-switching, the pulse duration is always longer than the roundtrip time, and repetition rate can be varied from a few hertz to a few Megahertz.

Q-switching is an excellent method to create powerful short laser pulses. But if ultra-short laser pulses are needed, we need to use other techniques.

1.1.2 Mode Locking

Another technique to create ultra-short laser pulses is mode locking. The mode-locking is based on constructive interference between different axial modes inside a laser cavity. Mode-locked lasers usually can generate pulses in picosecond to femtosecond regime. The energy in each pulse can be between micro joules to nano joules, and the repetition rate of these oscillators can be between Megahertz to Gigahertz.

To generate short laser pulses, we need to use a loss modulator in the laser resonator. The loss modulator should create a periodic loss which is matched to the roundtrip of the cavity. By doing this, the energy will be transferred to the longitudinal modes of our cavity, and the relative phase between the the longitudinal modes will not change. In other words, the phase will be locked. Then constructive interference can make an ultra-short laser pulse.

Just like Q-switching, the mode-locking methods can be divided into two groups: active and passive. In the active mode-locking, an electronic loss modulator is responsible for creation of a periodic loss. However, in the passive mode-locking a saturable absorber creates the loss. This absorber creates a high loss for low-intensity pulses. It allows only the pulses with high intensity to pass, and the recovery time of the saturable absorber should be lower than round trip time (because we want that one pulse to pass!). In a mode-locked laser, the pulse duration is always shorter than the roundtrip of the cavity, which will cause to have a pulse in the cavity at any moment. Moreover, the length of the cavity is the primary factor which determines the repetition rate of the oscillator.

Kerr lens mode-locking [8] is another passive way to make ultra-short laser pulses. These days the Ti:sapphire oscillators based on this technique can make pulses as short as five femtoseconds.

Kerr lens mode-locking (KLM) is based on Kerr effect. This effect is a nonlinear effect which can lead to changing of the refractive index of the medium. This change in refractive index will cause the medium to work as a lens for ultra-short laser pulses, which is called self-focusing. This self-focusing effect causes the material to works as saturable absorber, which eventually makes a periodic loss in the system. This effect is the basis of the Kerr lens mode-locking, which many these days' oscillators uses this principle to generate ultra-short laser pulses. [9]

Ti:sapphire crystal has a high nonlinearity and also a broad gain bandwidth. These two factors make this crystal the best candidate for generation of ultra-short laser pulses by Kerr lens mode-locking technique.

1.1.3 High Harmonic Generation

The main limitation to creating shorter laser pulses is the central frequency of a carrier wave. This central frequency will determine the temporal resolution of a pulse, which is the duration of one single optical cycle. This limitation explains why Ti:sapphire oscillators cannot make pulses shorter than five femtoseconds. To push the boundaries of ultrafast optics, we need to move to shorter wavelengths, and high harmonics generation(HHG) is one of the widely used ways to reach XUV and soft X-rays.

HHG can happen by focusing a very intense laser pulse into some specific gas (usually monoatomic gas like Neon or Argon). After that, the gas molecules will modulate the frequency of incident laser beam and generate odd harmonics of the incident beam. These harmonics can easily reach soft X-ray. This harmonic generation is a coherent process wherein these harmonics are highly correlated to each other. By correcting the phase of these harmonics it is possible to generate attosecond pulses. The world's shortest pulse generated by HHG up to date is 43 aottosecond. [10] HHG, however has a big drawback namely efficiency. This means that HHG cannot be used in many applications which need powerful pulses, and the output of HHG cannot be used for nonlinear experiments.

1.1.4 Multi Frequency Raman Generation

Multi frequency Raman generation (MRG) is a nonlinear technique to create single femtosecond laser pulses [11]. The temporal resolution of this technique is not comparable with HHG, but the energy of each pulse can be high (mJs), which will enable us to use MRG in areas that need intense pulses.

Just like the other short laser pulse generation methods, MRG also needs a broad spectrum. In the MRG, different Raman orders of a specific medium will be used to make a frequency comb from near IR to UV. This broad spectrum will enable us to create intense single-femtosecond pulses. The efficiency of MRG is much higher than HHG's, making MRG the best choice for applications that need intense short laser pulses.

MRG can be achieved by pumping a Raman medium using two powerful pumps coupled to the Raman transition of a specific medium. Stimulated Raman Theory can describe the process. The Raman medium can modulate the incident frequency and scatter the Stokes and anti-Stokes orders

[12]. This process can happen over and over again. These scattered orders can cover a broad spectrum.

All of the orders will be generated through a χ^3 process, which is the main reason for having higher efficiencies. Figure 1.1 shows the chain process of MRG, which eventually can make a broad spectrum.

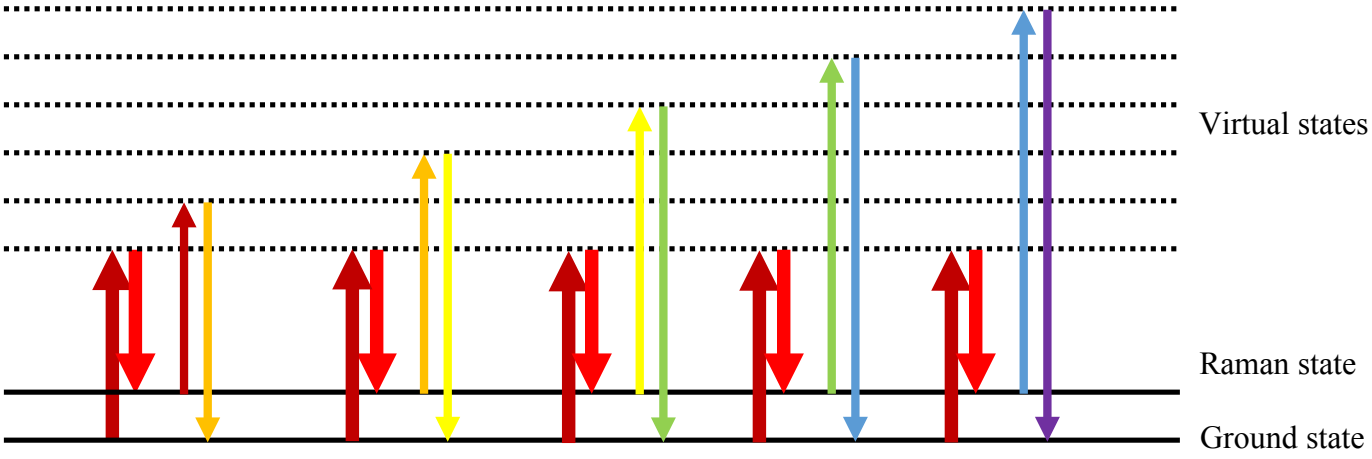

Figure 1.1 Energy level diagram for MRG

When the pumps intensity becomes sufficient, MRG can cover a broad spectrum

1.2 Literature Review of Pulse Compression Using Multiple Raman Orders

After the 90s, by using MRG, different techniques have been developed to create 1fs pulses. A good example of that has been done by Kung and his group [13]. They have used 2 nanosecond pulses of frequency ω_0 and $2\omega_0$, which were coupled to Raman state of H_2 molecules. This resulted in different phase locked Raman orders, which made a frequency comb. In this study, they used four prisms and one phase modulator to generate pulses as short as 850as.

Practically, MRG can be studied in three different temporal regimes. These regimes can be understood by comparing the dephasing time of the molecules (T_d) to the duration of the pump pulses (T_p). Dephasing time of the molecules is a function of the molecular collisions, which cause atoms not to act coherently [14]. In the adiabatic regimes, the pumps' duration is longer than the dephasing time ($T_p > T_d$). In the transient regime the dephasing time and pumps' durations are the same ($T_p \approx T_d$), however in the impulsive regime, the pumps duration is smaller than the dephasing time ($T_p < T_d$). A great review generation of ultra-short laser pulses by using Raman excitation has been written by Baker and his colleagues [11]. Further, the most important experiments in this field will be explained.

Harris and Sokolov have theoretically studied the MRG in the adiabatic regime [15]. The most important result of their theory is that the Raman orders can be phased. It means that the relative phase between the orders will not change. Then, by adding the orders together and temporally overlapping them, it is possible to make short laser pulses. They have also experimentally conducted an experiment to generate short laser pulses in the adiabatic regime. They used a four-prism delay line and a liquid crystal phase modulator to time the seven Raman orders, which were spanning from the 1.56 μm to 410 nm. After timing all the seven orders, they generated pulses with the temporal duration of 1.6 fs, pulse separation of 11 fs, and the peak power of 1 MW [16].

Katsuragawa and his group used a dual-wavelength injection-locked Ti:sapphire laser and liquid N_2 as the Raman active medium to adiabatically generate Raman orders. Finally, they used a setup base on chirp mirrors to time up all the Raman orders and generate pulses with the duration of 20 fs, repetition rate of 10.6 THz, and peak-power of 2 MW. The main drawback in the adiabatic regime is the low peak power of the generated pulses. Since, the repetition rate in this regime is

very high, the result is the pulses have low peak power, which eventually makes this technique not suitable for nonlinear experiments.

In order to have MRG in the impulsive regime we need to use pump pulses with the duration of a few-femtoseconds. Theoretical works and simulations have showed that in this regime it is possible to generate a broad spectrum to produce half-cycle-pulses [17]. But in practice, it has been shown that self phase modulation will happen and compete with Raman process, therefore, decreasing the efficiency of Raman generation [18] [19]. In order to avoid this problem, we can use another pulse with lower energy and delay. This can increase the efficiency of Raman generation without having self phase modulation [20] [21]. It has been predicted that this technique can generate spectrum, which is sufficient for producing 1fs pulses. Also by changing the injection time of the probe pulse, it is possible to be sure of arriving in phase, hence, causing to have good pulse compression [22] [23].

According to previous studies, researchers have shown that it is possible to generate 3.8fs pulses by exciting the Raman state of SF_6 gas [24] .Researchers have also showed that generating 23fs pulses is possible by using N_2 as Raman active medium [25]. The next studies in impulsive regime needs to generate wider spectrum. But because of the nonlinear interactions, this generation can not be simply done by increasing the energy of the input pump pulses.

Comparing to transient and adiabatic regime impulsive MRG is not suitable for generating ultra-short laser pulses. The main reason is that in this regime the interaction between the SPM and the MRG will effect the final output spectrum [26]. Also, as previously mentioned, it is not possible to generate pulses with high peak power in the adiabatic regime.

The next regime for studying MRG is transient regime. MRG in the transit regime was first observed by Irie and Imasaka through using the H_2 as the Raman active medium and a UV excimer laser as a single pump [27]. Sali and his colleagues has also shown that by using two color pumping in the transient regime, it is possible to generate a wide spectrum in both H_2 and CH_4 [28].

Now we can mention the advantages of generation of Raman orders in transient regime. MRG in the transient regime has many advantages to generate ultra-short laser pulses with high peak power. In this regime, it is possible to avoid the SPM affect and generate a wide spectrum, but generating ultra-short laser pulses in this regime needs special care on phasing the Raman orders. Not only it

is required to time up the orders, there is the need of phase locking the orders by compressing each order to its Fourier transform limited pulse durations.

Sokolov has studied generation of short laser pulses in the adiabatic regime. They have pumped D_2 cell by using Nd: YAG and Ti:sapphire laser. Further, they have used a single prism and a few tilted glass plates to time all of the orders to get a short laser pulse. [29]

Our following research in this thesis is in transient regime. The short term goal of this research is to compress the first anti-Stokes order by using a simple prism compressor. The long term goal of this research is to compress the other orders and time up the orders to generate single-femtosecond pulses.

1.3 Introduction of the Experimental Section.

In our lab, the MRG have been studied in the transient regime, which can provide maximum numbers of coherent orders [30].

The Raman media can be chosen from different liquids, solids, and gases samples [31], but the H_2 is the most common material which has been used for the generation of different Raman orders. The main reason for choosing the H_2 is the simplicity. H_2 is not an expensive material, can be available in the pure format, and many other reasons made this gas an excellent candidate for MRG. In our lab, we use Sulfur hexafluoride (SF_6) for generating different Raman orders, and the main reason that we use this gas is that the Raman frequency of this gas is matched with the laser setup that we have in our lab. We use a dual wavelength Ti:Sapphire CPA system for generating the two pumps. The frequency separation between these two pumps can be set to 23.25 THz to resonate with the Raman frequency of Sulfur hexafluoride (SF_6).

To avoid self-phase modulation (SPM), we leave a linear chirp on the each of the pumps. This can be easily done by placing the grating in front of the optimum place. One of the back mirrors in the Grating compressor is placed on a portable stage, which will enable us to control the delay between the pumps, and to change the instantaneous frequency between the two pumps. After the grating compressor, the two pump pulses with the total energy of 1.5mj will be directed to the hollow fiber, which is filled with SF_6 gas. After the fiber, we have different Raman orders, which are spread from the infrared to the UV. Our Raman orders are highly correlated to the pumps. They will have the same chirp as the pumps have. The final step is using a pulse compression system to compress the first Raman order.

1.3.1 Research Goal

Because we are studying the MRG in the transient regime, all the Raman orders and the pumps are coherent and can be coherently added together. To add all the different orders together, the phase of the orders should be corrected. Our pulse compression system can do this. By using two prisms pair pulse compression system, we have successfully compressed the first anti-stokes order to its Fourier's transform limit, which is around 300fs.

By changing the delay between the two chirped pumps, we can change the instantaneous frequency separation between them. This change in the instantaneous frequency can cause red-shifting for the Raman orders [32]. Figure 1.3 shows the spectrum with and without red-shifted shoulders. We do not have any theoretical description for this process, but we think that this effect can be beneficial because we can change the frequency spacing between the Raman orders. By changing the spacing, we can have fewer pulses in our final pulse train, which means the final output power can be increased significantly.

In this thesis, we use our pulse compression system to compress and study the phase behavior of the first anti-Stokes order in the presence of the red-shifted spectrum.

(a)

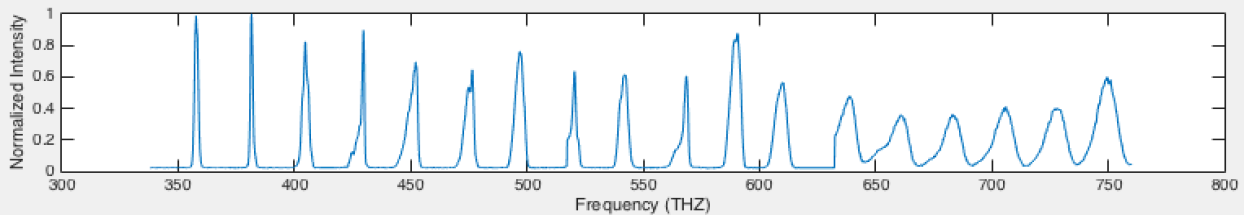

(b)

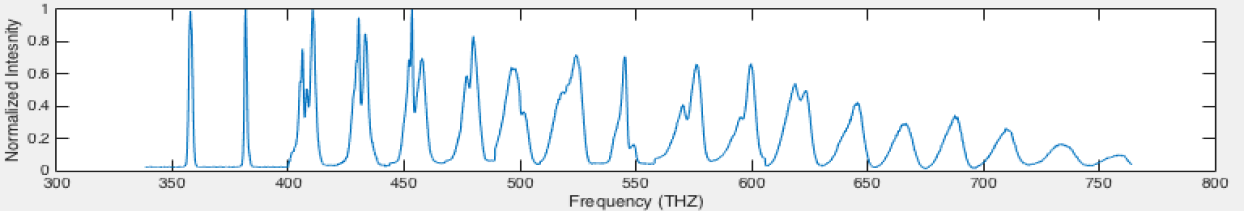

Figure 1.2: Measured MRG spectrum. (a)without red-shifted shoulders (b)with red-shifted shoulders

Chapter 2

Theory & Background

2.1 Description of Short Laser Pulses

In order to describe a short laser pulse, let us first start by describing a plane monochromatic wave. We have the Maxwell wave equation:

$$\frac{\partial^2 E}{\partial z^2} - \frac{1}{c}\frac{\partial^2 E}{\partial t^2} = 0 \tag{2.1}$$

The solution for this equation is a plane monochromatic wave.

$$E(t,z) = E_0 e^{i(\omega_0 t - kz)} + cc \tag{2.2}$$

Equation 2.2 describe the nature of a plane wave, which has one frequency. In the real world there is not any source, which can produce monochromatic light waves. All of the light waves have a limited bandwidth, which does not allow them to be a single frequency. But, in many cases the bandwidth for a CW laser is negligible. For example, a typical He-Neon laser has the bandwidth of 0.002nm, which is very small and can be called monochromatic.
In order to describe a CW laser pulse, we also need to solve the Helmholtz equation, which is:

$$(\nabla^2 + k^2)E(x,y,z) = 0 \tag{2.3}$$

The solution for equation 2.3, provides us the general representation of a Gaussian laser beam, which is:

$$E(x,y,z) = I_0 e^{\left[-\frac{x^2+y^2}{\omega^2(z)}\right]} e^{\left[-i\frac{k(x^2+y^2)}{2R(z)}\right]} e^{[-ikz-\varphi(z)]} + cc \tag{2.4}$$

where $\omega(z)$ is the spot radius at z

$$\omega(z) = \omega_0 \sqrt{1 + \left(\frac{z}{z_R}\right)^2} \tag{2.5}$$

R(z) is the curvature of the wave fronts, which is:

$$R(z) = z\left[1 + \left(\frac{z}{z_R}\right)^2\right] \tag{2.6}$$

φ(z) is phase shift where:

$$\varphi(z) = arctg(\frac{z}{z_R}) \tag{2.7}$$

We can also add the temporal phase term to the E field equation, then the final equation for a CW laser pulse will be:

$$E(x,y,z,t) = \sqrt{I_0}\, e^{[-\frac{x^2+y^2}{\omega^2(z)}]}\, e^{[-i\frac{k(x^2+y^2)}{2R(z)}]} e^{[i(\omega_0 t - kz + \varphi(z) + \varphi(t))]} + cc \tag{2.8}$$

Short laser pulses have a broad spectrum, which will determine the duration of the transform limited pulse. For describing a short laser pulse, we also need to add a temporal term, which normally is also a Gaussian function. Then, we can describe it as follows:

$$E(x,y,z,t) = \sqrt{I_0}\, e^{-\left(\frac{t}{t_p}\right)^2}\, e^{[-\frac{x^2+y^2}{\omega^2(z)}]}\, e^{[-i\frac{k(x^2+y^2)}{2R(z)}]} e^{[i(\omega_0 t - kz + \varphi(z) - \varphi(t))]} + cc \tag{2.9}$$

where ω_0 is the carrier frequency of the pulse.

Description of Pulse in Temporal Domain:

As we can see in equation 2.9, the description of short laser pulses is very complicated. Then, for simplicity we just look at the temporal profile of the pulse. We also ignore the complex conjugate term for simplicity. After all of these simplifications, the complex field will be:

$$E(t) = \sqrt{I(t)}\, e^{i(\omega_0 t - \varphi(t))} \tag{2.10}$$

Which ω_0 is carrier frequency of the pulse.

Description of Pulse in Frequency Domain:

In many cases, it easier to describe a pulse in the frequency domain. By using Fourier transformation, we can move from temporal to frequency domain. Then we have:

$$E(\omega) = \frac{1}{2\pi}\int_{-\infty}^{+\infty} E(t)e^{-i\omega t}\,dt \tag{2.11}$$

Then, we can write the electric field as follows:

$$E(\omega) = \sqrt{S(\omega)}e^{i\phi(\omega)} \tag{2.12}$$

Where $\phi(\omega)$ is called spectral phase, and $S(\omega)$ is called spectrum, which will be measured by the spectrometer. By using the frequency domain definition of a pulse, we can more easily describe the propagation of a pulse inside a medium, which will be discussed in the next section

2.2.1 Dispersion:

Dispersion in optics is based on the dependence of refractive index on the frequency. This will cause waves with different frequencies to face different speeds in the medium. In the ultra-fast optics, controlling the dispersion is crucial because short laser pulses have a relatively large bandwidth. Then, different colors have different speeds, which will cause broadening of the pulse. So, it is important to have full control on the dispersion in ultra-fast optics. The following picture shows the dependence of refractive index of SF10 glass on frequency:

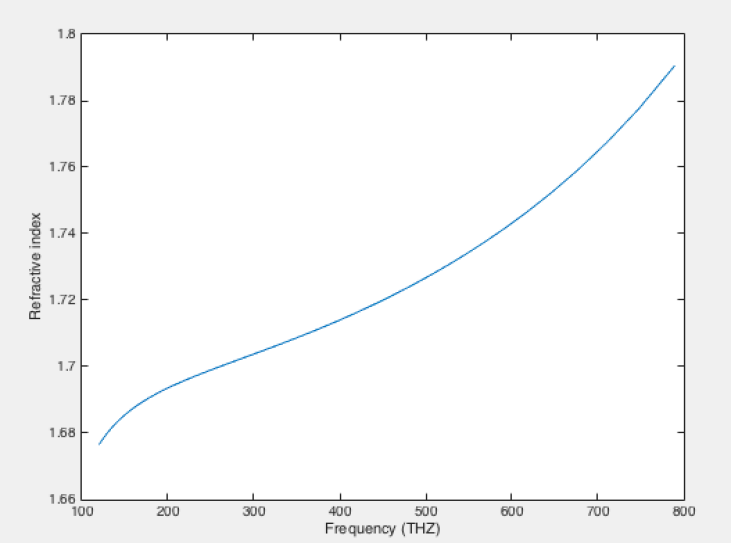

Figure 2.1: refractive index of SF10 as the function of frequency [33]

As we can see in the last picture, in a normal dispersion region, the refractive index will increase with frequency. The Sellmeier equation will describe this dependence of [34]:

$$n^2(\lambda) = 1 + \sum_i \frac{B_i \lambda^2}{C_i - \lambda^2} \tag{2.13}$$

where C_i, and B_i are the Sellmeier coefficients. This equation shows that different materials can have different electronic response to the different frequencies. The following table shows the Sellmeier coefficients for four different materials [34]:

	B_1	B_2	$C_1(\mu m)$	$C_2(\mu m)$
SF10	1.616259	0.2592293	0.01275345	0.05819839
BK7	1.039612	0.2317923	0.006000698	0.02001791
Fused silica	0.696166	0.4079426	0.004679148	0.01351206
BAK1	1.1236566	0.3092768	0.006447427	0.02222844

Table 2.2: The Sellmeier coefficients for four different glass

When a pulse enters a medium with dispersion, after passing the length L it will face a change of spectral phase change, which is:

$$\Delta\phi(\omega) = \frac{\omega}{c} n(\omega) L \tag{2.14}$$

Another approach to describe the change of spectral phase of a pulse is using the Taylor expansion around carrier frequency ω_0:

$$\phi(\omega) = \phi_0 + \frac{d\phi}{d\omega}(\omega - \omega_0) + \frac{1}{2}\frac{d^2\phi}{d\omega^2}(\omega - \omega_0)^2 + \frac{1}{6}\frac{d^3\phi}{d\omega^3}(\omega - \omega_0)^3 + \cdots \tag{2.15}$$

The first term, ϕ_0, is called the absolute phase, which describes the exact phase of the carrier frequency. The second term, $\frac{d\phi}{d\omega}$, which is the first derivative of the spectral phase, is group

velocity. The third term, $\frac{d^2\phi}{d\omega^2}$, is called the group delay dispersion(GDD), the fourth term which is the third derivative of the phase is called the third order dispersion(TOD), and so on.

ϕ_0 and $\frac{d\phi}{d\omega}$ do not have any effect on the shape of a short pulse. $\frac{d\phi}{d\omega}$ is also called group delay, which only causes the delay in time. But GDD, TOD and other orders have very important impacts on the behavior of a short pulse.

Generally, when we have laser pulses as short as 100 fs, the GDD plays the key role and needs to be considered, and compensated if needed. If we have pulses as short as 30fs, the TOD also needs to be considered, and if we have pulses less than 10fs, higher orders also need to be considered.

When we have a short pulse with only the absolute phase, we call it transform limited pulse. For example, the following picture shows a 10 fs transform limited pulse.

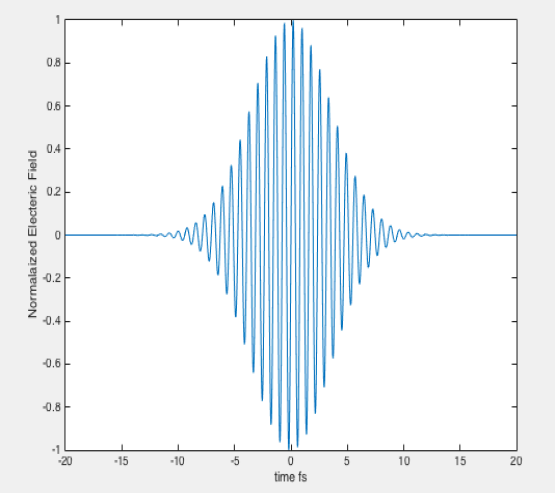

Figure 2.2 The electric field of a Gaussian pulse with flat temporal phase

For a Gaussian transform limited pulse, we have the following relation between the frequency bandwidth and the minimum pulse duration:

$$\Delta\nu\Delta t = \frac{2ln2}{\pi} \tag{2.16}$$

This equation shows how short our our pulse can be for a given spectrum. For example, in order to have 10 fs pulse, we need to have at least 100 nm bandwidth centered at 800nm, which is on practice achievable by using a Ti:sapphire crystal.

Adding different GDD, TOD, and higher order dispersion will significantly change the temporal shape of the pulse. For example, adding the GDD to 10 fs pulse will cause the pulse to be broader. In practice, the broadening of an optical pulse inside an optical medium is function of group velocity mismatch multiply the length of optical path, which is called GDD. The following picture shows how a 10 fs pulse will change by adding just GDD.

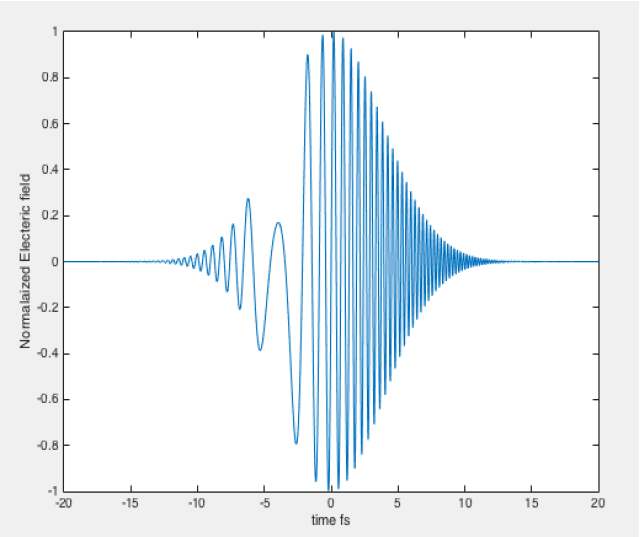

Figure 2.3 The electric field of a Gaussian pulse with quadratic temporal phase

Now the question is how does the duration of the pulse change by adding a known amount of GDD. If we have a Gaussian shape pulse, the following equation predict the final pulse duration after by adding a known GDD:

$$\frac{\tau_{\mathrm{f}}}{\tau_o} = \sqrt{1 + \left(\frac{4ln2 \times GDD}{\tau_0^2}\right)^2} \tag{2.17}$$

where τ_o is the initial pulse duration, and τ_{f} is the final pulse duration.

2.2.2 Material Dispersion (Group Delay Dispersion):

When a short laser pulse passes through a medium, different colours will be separated. This is mainly because of group velocity mismatch between different colours. Normally, group velocity will increase by increasing wavelength. Then the head of the pulse will be shifted to the red, and the tail of the pulse will be shifted to the blue.

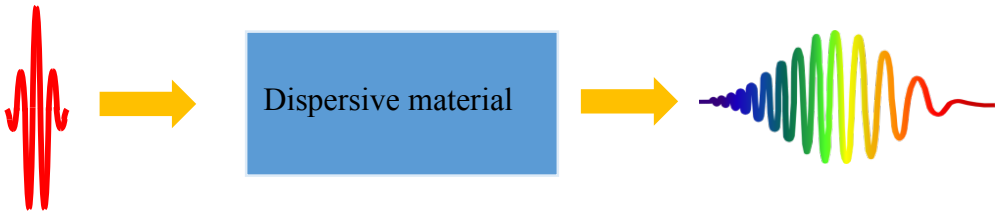

Figure 2.4: Broadening of a laser pulse by propagation through a dispersive material

To understand the exact effect of dispersion on short laser pulses, we need to get back to equation 2.18 which is:

$$\phi(\omega) = \phi_0 + \frac{d\phi}{d\omega}(\omega - \omega_0) + \frac{1}{2}\frac{d^2\phi}{d\omega^2}(\omega - \omega_0)^2 + \frac{1}{6}\frac{d^3\phi}{d\omega^3}(\omega - \omega_0)^3 + \cdots \tag{2.18}$$

In order to calculate the different derivatives when our pulse is passing through the medium with the length of L, we can write the spectral phase as follows:

$$\phi(\omega) = k(\omega)L \tag{2.19}$$

Then, we can easily calculate different derivatives of the spectral phase. After some calculation, we have the following equations for different derivatives [35]:

$$\frac{d\phi}{d\omega} = L\frac{d}{d\omega}k(\omega) = \frac{L}{v_g} \equiv Group\ delay \tag{2.20}$$

$$\frac{d^2\phi}{d\omega^2} = L\frac{d^2}{d\omega^2}k(\omega) = L\frac{\lambda^3}{2\pi c^2}\frac{d^2n(\lambda)}{d\lambda^2} \equiv Group\ delay\ dispersion(GDD) \tag{2.21}$$

$$\frac{d^3\phi}{d\omega^3} = L\frac{\lambda^4}{4\pi c^3}\left(3\frac{d^2n(\lambda)}{d\lambda^2} + \lambda\frac{d^3n(\lambda)}{d\lambda^3}\right) \equiv Third\ order\ dispersion(TOD) \tag{2.22}$$

2.2.3 Dispersion Compensation

As we have mentioned before, dispersion can affect the temporal profile of a short laser pulse. Different dispersion orders have different effects on the temporal behavior of a pulse.

Dispersion in the short laser pulses usually can be compensated by changing the optical path for different colors. There are many different setups to do that: Prisms, grating, chirped mirror, spatial light modulators, etc. However, prism ad grating setups are the most common solution for controlling the dispersion. Now we review the basic concepts of grating and prism compressors in this chapter.

2.2.3.1 Grating Compressor

Treacy grating pair:

Treacy was the first one who have shown that two parallel gratings can be used to introduce negative dispersion [36]. Since then different setups of grating pairs have been used to control dispersion in the field of ultra fast optics. The most common setup is shown in the figure 2.5. Two parallel gratings and one back mirror can be used to introduce negative dispersion for compressing a pulse. The phase of the grating compressor will be [35]:

$$\phi_{Grating}(\omega) = \frac{4\omega\, G\, sec\theta_D}{c}\left[1 - \left(\frac{2\pi c}{\omega d} - sin\theta_i\right)^2\right]^{\frac{1}{2}} \tag{2.23}$$

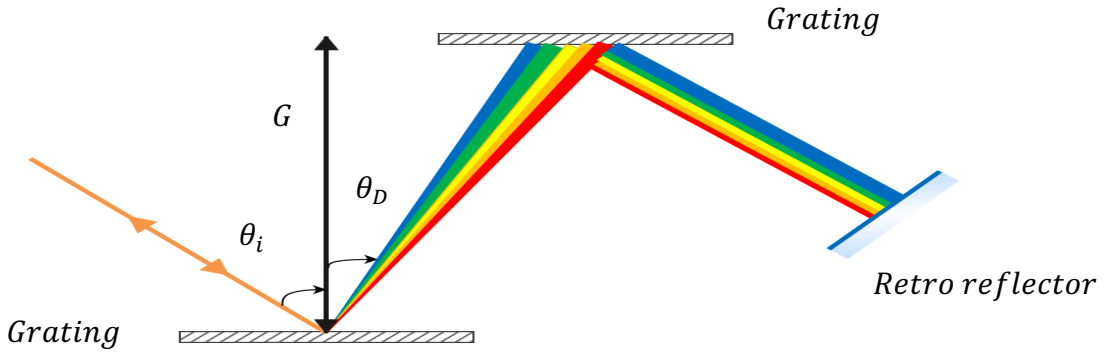

Figure 2.5: Treacy grating pair setup

Where G is the separation between the gratings, d is the grating period, and θ_i is the incident angle. The second and third order dispersion of the grating can be easily calculated and will be as follows [24]:

$$\frac{\partial^2\phi}{\partial\omega^2} = \frac{\lambda^3\, G\, sec\theta_D}{\pi c^2 d^2 \cos^2\theta_D} \equiv Group\ delay\ dispersion(GDD) \tag{2.24}$$

$$\frac{\partial^3\phi}{\partial\omega^3} = \frac{-3\lambda^4\, G\, sec\theta_D}{2\pi^2 c^3 d^2 \cos^2\theta_D}\left[1 + \frac{\lambda}{d}\frac{sin\theta_D}{\cos^2\theta_D}\right] \equiv Third\ order\ dispersion(TOD) \tag{2.25}$$

As we can see GDD is always negative, and TOD is always positive for this grating pair.

Grating pair with internal lenses:

Another way to use gratings for dispersion compensation is to use two gratings and two lenses to make a pulse compressor or stretcher [37] [38]. Figure 2.6 shows this setup. In this setup, the dispersion can easily be controlled by changing the distance between the gratings ($l_1 + l_2$). If the $l_1 + l_2 > 0$, the setup works as a stretcher. If the the $l_1 + l_2$<0, the setup works as a compressor, and finally if the $l_1 + l_2 = 0$,it can be used as a pulse shaper.

The second order dispersion of this system (GDD) is given by [35]:

$$\frac{\partial^2\phi}{\partial\omega^2} = \frac{\lambda^3(l_1 + l_2)}{\pi c^2 d^2 \cos^2\theta_D} \tag{2.26}$$

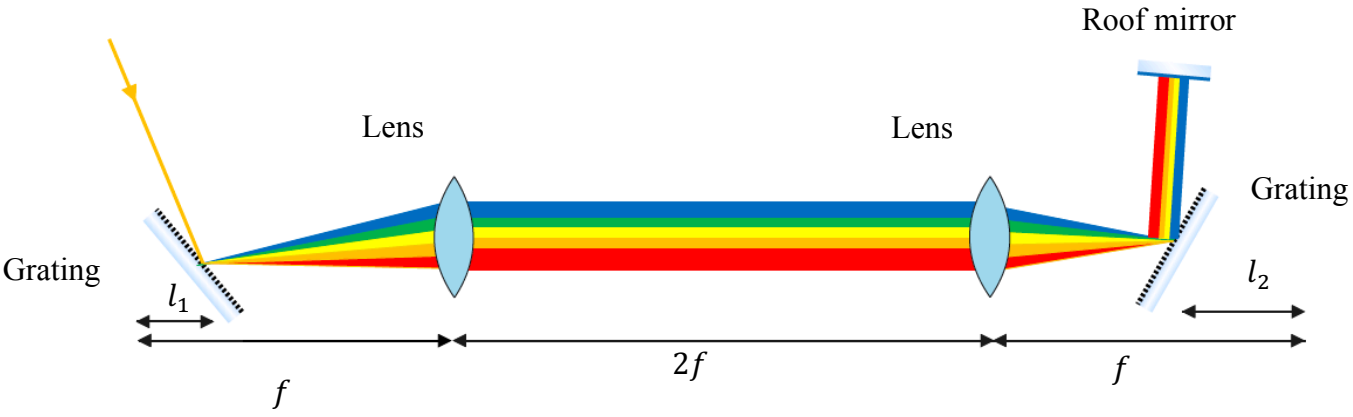

Figure 2.6: Grating pair setup with two internal lenses

2.2.3.2 Prism Compressor

Prisms are another technique for providing angular dispersion, which are widely usable in ultrafast optics as a dispersion compensation technique [39]. Prism pairs have their own advantages and disadvantages for dispersion controlling. The main advantage of prism pair is that they have low loss, which makes them an excellent choice for controlling the dispersion inside a laser resonator. On the other hand, compared to grating pairs, prism pairs provided a very limited angular dispersion, which is their main disadvantage. Then, in order to have a high GDD, the separation between the prisms should be increased, which is not possible in some applications.

The final dispersion term of a prism pair has two different terms, one of them is coming from the material dispersion, which has a positive sign, and the other term is coming from the angular dispersion, which has a negative sign. This will make it easier to tune the dispersion of a pulse by using prims pairs.

To have pulse compression systems working in their best condition, special care for alignment is needed. Usually, we use the minimum deviation angle for aligning the prism compressor systems. The result of using the minimum deviation angle is that the beam path will be symmetric. So, the incident angle and the exit angle will be the same. This makes the tuning very easy because by moving the prisms perpendicular to the beam path, the exit angle will not be changed. Then, this vertical movement does not have any effect on the misalignment of the beam; but, we can use it to control the amount of the glass in the beam path, which means tuning the GDD. The following picture, shows a prism in the minimum deviation condition:

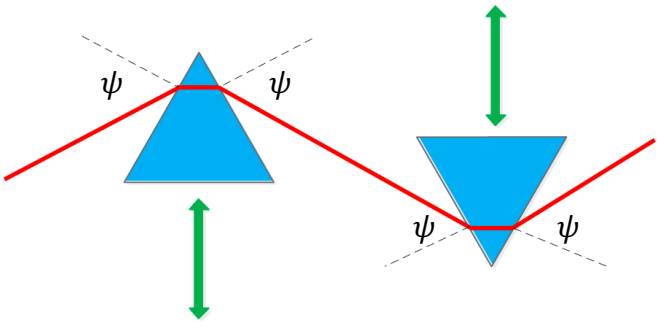

Figure 2.7: Prism sequence for dispersion control in the minimum deviation condition. In this condition the, perpendicular movement of the prisms does not change the beam path.[15]

We also know that the minimum deviation angle is a function of the apex angle. Then, by choosing the apex angle wisely, the incident angle and exit angle can satisfy the Brewster condition. This will significantly reduce the loss of the whole system. (This is the main reason that P polarized beam will face a low loss in the prisms)

The following equations will provide the second and third order dispersion of a prisms pair system [35]:

$$\frac{\partial^2\phi}{\partial\omega^2} = \frac{\lambda^3}{2\pi c^2}\left\{4L_{sep}\left(\frac{dn}{d\lambda}\right)^2 - 2L_{glass}\left[\frac{d^2n}{d\lambda^2} + \left(2n - \frac{1}{n^3}\right)\right]\right\} \tag{2.27}$$

$$\frac{\partial^3\phi}{\partial\omega^3} = \frac{\lambda^4}{\pi^2 c^3}\left\{6L_{sep}\left(\frac{dn}{d\lambda}\right)^2 - \frac{1}{2}L_{glass}\frac{d^2n}{d\lambda^2}\right\} \tag{2.28}$$

Where L_{sep} is the distance between the two prisms, and L_{glass} is the length of the beam path inside the material.As we have mentioned before, the second and the third order dispersion of the prisms each have two terms with different signs, which make the prism pairs an easy option for tuning the dispersion. There are different setups for prism compressors. These different setups have one thing in common, which is the beam should pass through the prisms four times to minimize the special chirp in the output. The following pictures, show the different setups for prism pairs [40]:

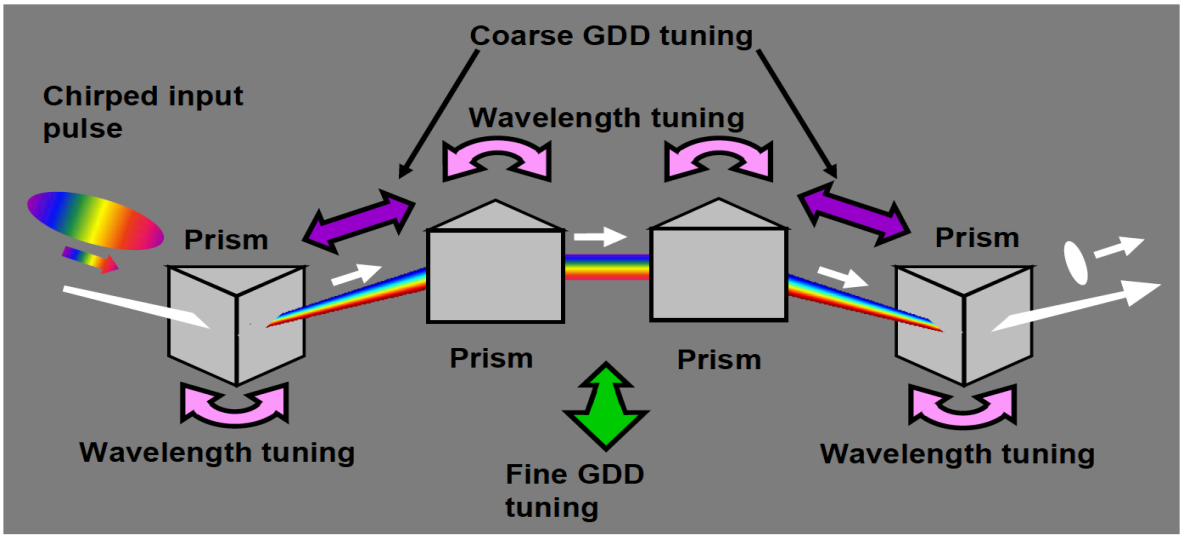

Figure 2.8: Four prism compressor setup [40]

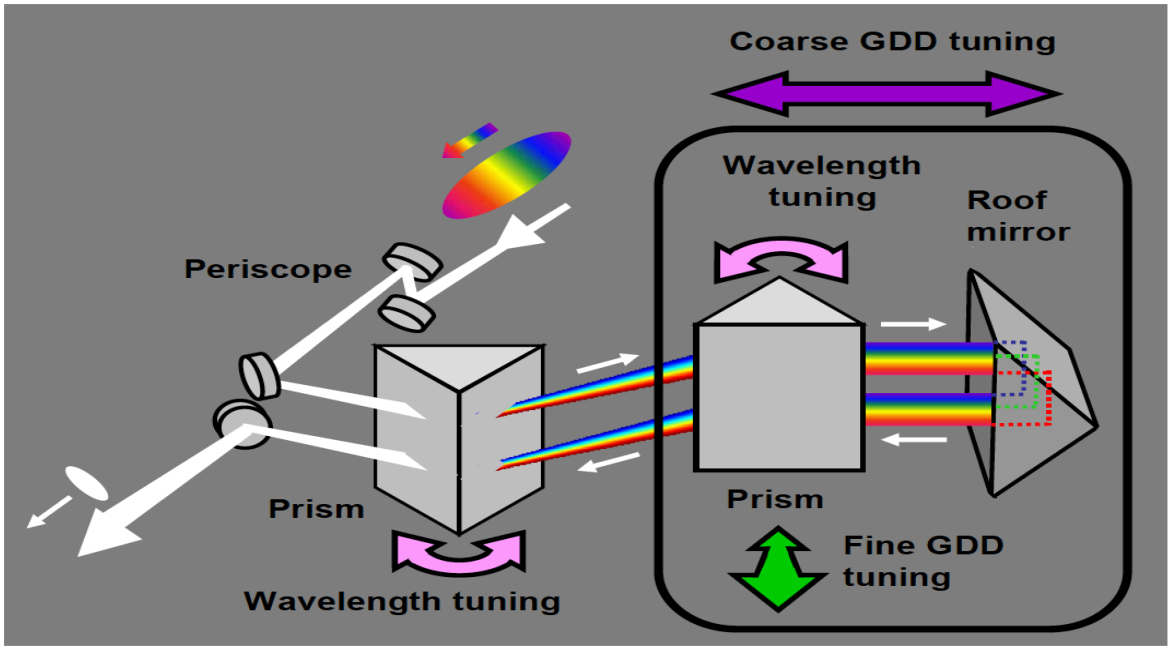

Figure 2.12: Double prism compressor setup [40]

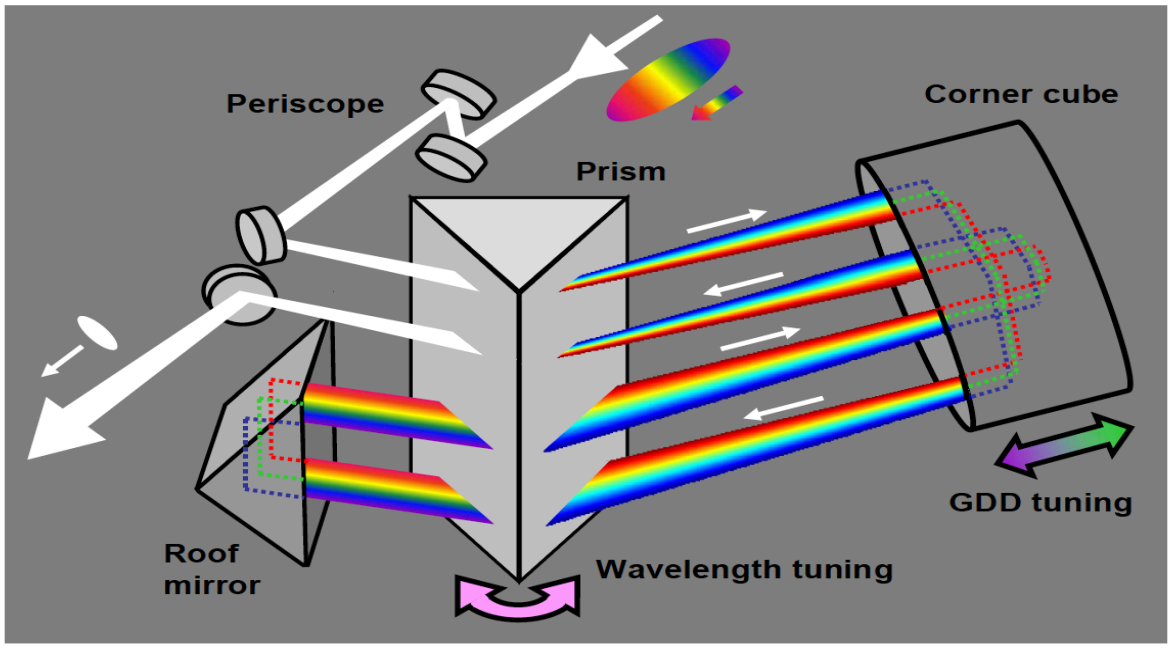

Figure 2.13: Single prism compressor setup [40]

2.3 Ultra-short Pulse Measurement and Correlation Technique

In the field of ultrafast optics, it is critical to have enough information about the temporal and the spectral profile of a pulse. There is a solid connection between the spectrum and the duration of a pulse. As we have mentioned before, for a Gaussian transform-limited pulse, we have the following relation between the frequency bandwidth and the minimum pulse duration:

$$\Delta\nu\Delta t = \frac{2ln2}{\pi} \tag{2.29}$$

However, this equation is only valid for transform-limited pulses. If our pulse has higher order dispersion terms (like second order dispersion), the pulse will be broader. Then, the equation 2.29 cannot describe the temporal behavior of our pulse. So, in this case, the spectrometer is not enough to reveal information about the temporal behavior of a pulse. We need to measure the pulse duration with other techniques.

Moreover, the laser pulses in the femtosecond regime are much faster than the temporal response of the electronics device. Then it is not possible to use oscilloscopes and photodiodes to measure the duration of ultrashort laser pulses. In order to measure the pulses in the femtosecond and attosecond regime, we can use a copy of a pulse as a gating function to get more information. This will be the basic concept of the autocorrelation technique.

In our lab, we are using a single shot autocorrelation setup to measure the temporal profile of a pulse. In section 3.3, we have explained this technique's setup in detail. So, in this section we only review the basic concepts of the intensity autocorrelation theory.

In this method, we use a beam splitter to divide a pulse into two separate copies. By giving a delay to one of the pulses, they can spatially overlap inside a nonlinear medium. This can eventually cause to have nonlinear interaction such as the second harmonic generation (if the phase matching condition is satisfied). The intensity of the SHG pulse will be a function of the time delay between the pulses. The SHG's intensity will be as follows:

$$I_{SHG}(\tau) \propto I(t)I(t-\tau) \tag{2.30}$$

However, the electronic devices are too slow to measure the temporal behavior of the SHG' intensity. But, they can measure the intensity autocorrelation, which can be defined as follows:

$$A^2(\tau) = \int_{-\infty}^{+\infty} I(t)I(t-\tau)dt \tag{2.31}$$

It is clear that SHG generation can only happen if the two pulses are overlapping in time. Then, the intensity autocorrelation is a function of the temporal profile of the pulse.

So, the question is that what kinds of information we can get from the intensity autocorrelation of two optical pulses? It is clear that if the delay between the pulses be zero, the autocorrelation function has its maximum. Also, if the two pulses do not have any overlap, the autocorrelation function will be zero. Autocorrelation has its ambiguities. The main three ambiguities are the direction of time, spectral phase information, and finally the unity of the results. Now, let us explain these ambiguities.

The first ambiguity, direction of time, means that a pulse and its time reversal copy have the same autocorrelation. The second ambiguity, spectral phase information, means that we cannot extract any information about the exact spectral phase of a pulse. The only information that we can get is to use the time-bandwidth equation, $\boldsymbol{\Delta\nu\Delta t = \frac{2ln2}{\pi}}$, to calculate the duration of the limited transform pulse. If our measured autocorrelation gives us the same result, then we can say that the pulse' spectral phase does not have any second or higher order terms.

The third ambiguity, unity of the results, means that different pulses with different intensities can have the same intensity autocorrelation curves, which makes the de-convolution impossible in some cases (even Tom Cruise from the Mission Impossible movies cannot make it possible) [41]. This is one of the most significant drawbacks of the autocorrelation technique, but in our experiment, it does not affect our results because we do not use any pulse shaper in our laser setup. Then, we can assume that our laser pulses have a simple Gaussian shape profile (I would like to confess that this assumption made my life much more comfortable in the last two years).

Now, the question is that what is the exact relationship between the autocorrelation curve and the intensity profile of the pulse? The answer is: if we have a Gaussian shape pulse, the FWHM of an autocorrelation curve is 1.4 times wider than the FWHM of the intensity profile of the pulse.

Chapter 3

Experimental Setups:

3.1 Dual Wavelength CPA System:

Figure 3.1 shows the overview of the experimental setup for our project. Our setup is based on a dual wavelength CPA system, which will provide us with two pump pulses [42]. The pump pulses are centered at 786 nm and 836nm, which is perfectly matched with the Raman transition of SF_6 gas. We are using SF_6 to generate Raman orders for two reasons. The first one is that the spacing between the Raman states of this specific gas matches with the experimental laser setup that we have in the lab. The other reason is that the frequency spacing between the Raman orders of SF_6 is relatively small, which will enable us to have fewer single-femtosecond pulses in the final pulse train with high peak power as the output.

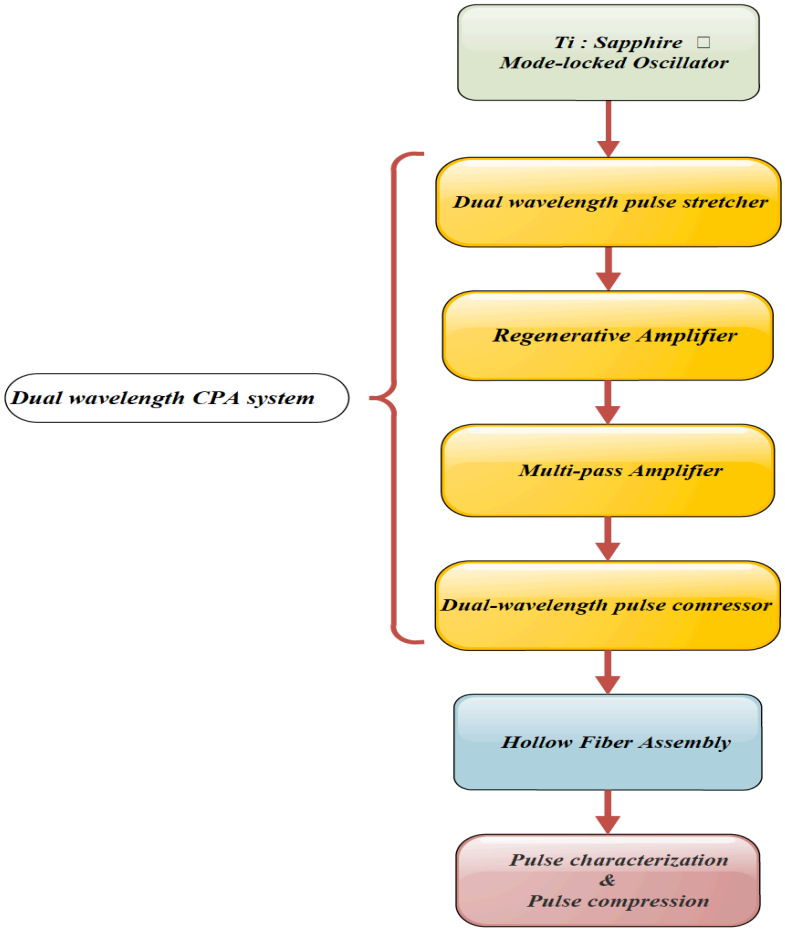

Figure 3.1: Flowchart of our experimental setup

3.1.1 Femtosecond Oscillator

As the primary source for the seeding of our CPA system, we are using a commercial Kerr-lens mode-locked Ti:Sapphire oscillator (FEMTOLASER Scientific PRO).

This oscillator is shared with Dr. J. Sanderson's lab. It generates 10 fs pulses with a central wavelength of 800nm. The repetition rate of the oscillator is 75 MHz, and the average power is 400mW. We are using a beam splitter and direct 50% of the oscillator's output power to our lab by using a 30m optical fiber. This beam will be used for seeding our CPA system to generate two distinct pump pulses. Figure 3.2 shows the measured spectrum of our oscillator and figure 3.3 shows the inside cavity of this oscillator.

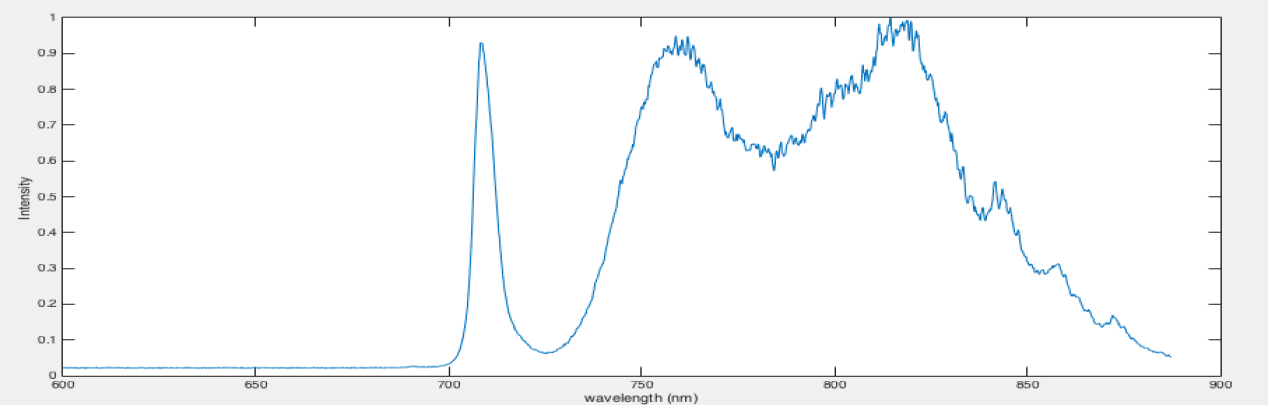

Figure 3.2: Measured spectrum of the oscillator

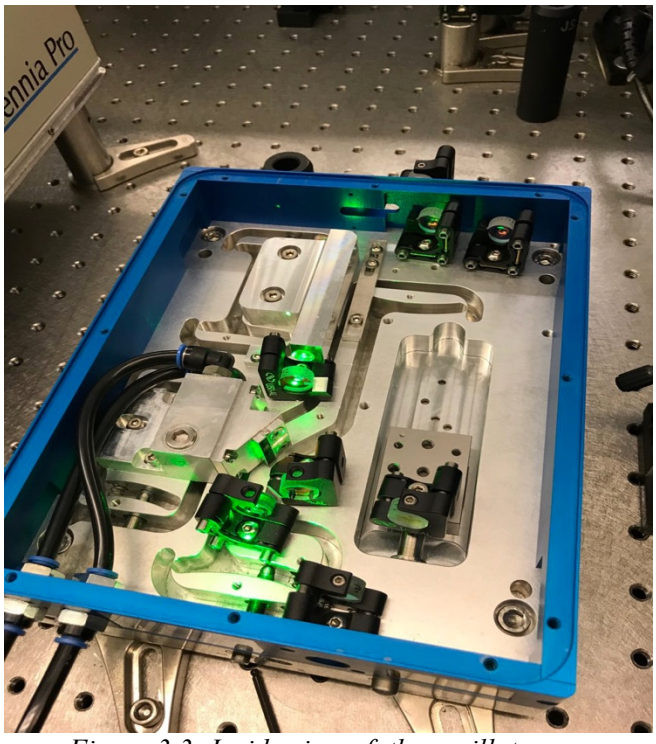

Figure 3.3: Inside view of the oscillator

3.1.2 Dual Wavelength Pulse Stretcher

The first stage of any CPA system is stretching the pulse. After the oscillator, we have a 30 m long optical fiber and a pulse stretcher to broaden the pulse from 10 fs to 1ns. Figure 3.4 shows the setup of our stretcher. We have used a prism pair, grating, and a concave mirror to build this stretcher (Martinez-type stretcher) [43]. This stretcher also works as a frequency filter. By changing the position of the two back prisms, we can select the specific parts of the spectrum to be stretched and directed to the Regenerative amplifier.

Our stretcher is equivalent to the "two grating and two lenses" stretcher. In our setup, we use a concave mirror instead of the lens for simplicity. Figure 3.5 shows the spectrum of the seeding beam after being filtered and stretched.

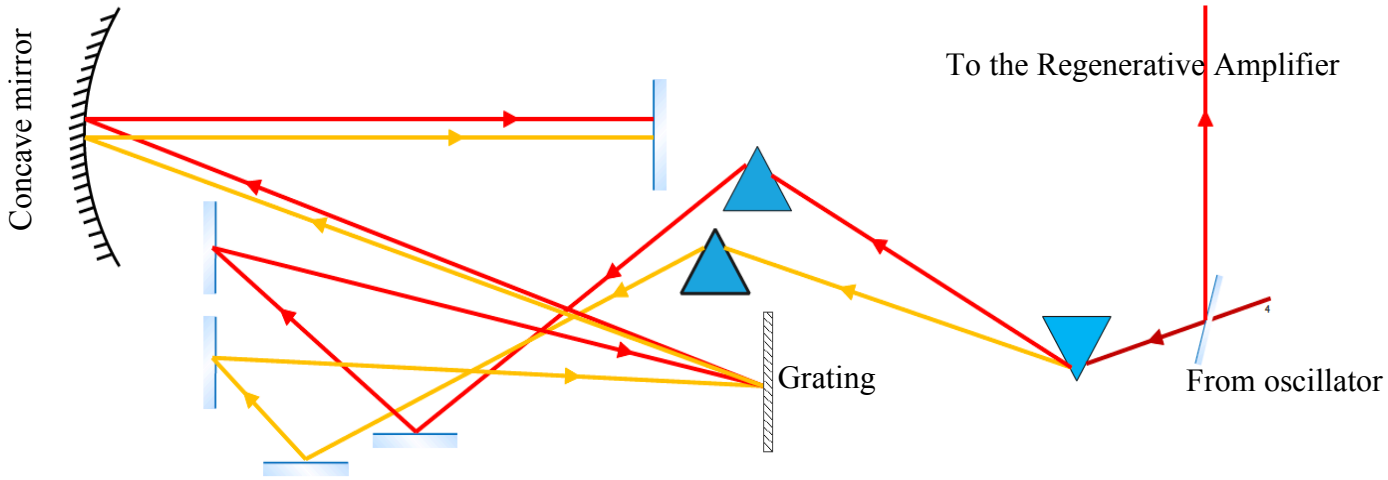

Figure 3.4: Pulse stretcher setup

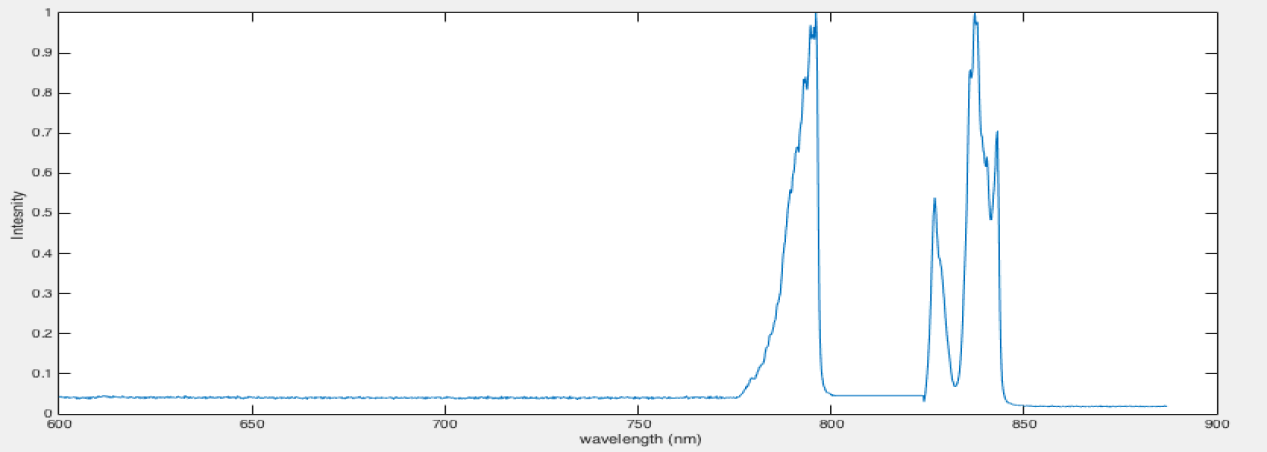

Figure 3.5: Measured spectrum of the seed beam after stretcher

3.1.3 Regenerative Amplifier

The most important part of our Dual-Wavelength CPA system is the Regenerative amplifier. Then, the alignment of this part plays a significant role in the total performance of the whole system and needs special care. This Regen is designed to only amplify two specific narrow part of the spectrum. Figure 3.6 shows the design of this amplifier, which we have made in our lab.

We use the output of the pulse stretcher for seeding this Regen. Our Regen is an X shaped cavity with four mirrors. Two of the mirrors are concave mirrors enabling us to have a stable cavity. We also use two prism pairs inside the Regen cavity, designed to separate the two seeding beams, and control the exact spectrum of each of them. By having two slits after the prisms, we have the full control of the bandwidth of each wavelength. Usually, we set the bandwidth of each pump to around 3 nm. The long wavelength is centered at 837 nm, and the shorter one is centered at 786nm. The gain medium inside our cavity is a Ti: Sapphire crystal, which matches our oscillator's crystal.. We use a Q-switched Nd: YAG laser from Spectra-Physics to pump the crystal. The output of this laser is 532nm, which is perfectly matched with the absorption spectrum of our gain medium.

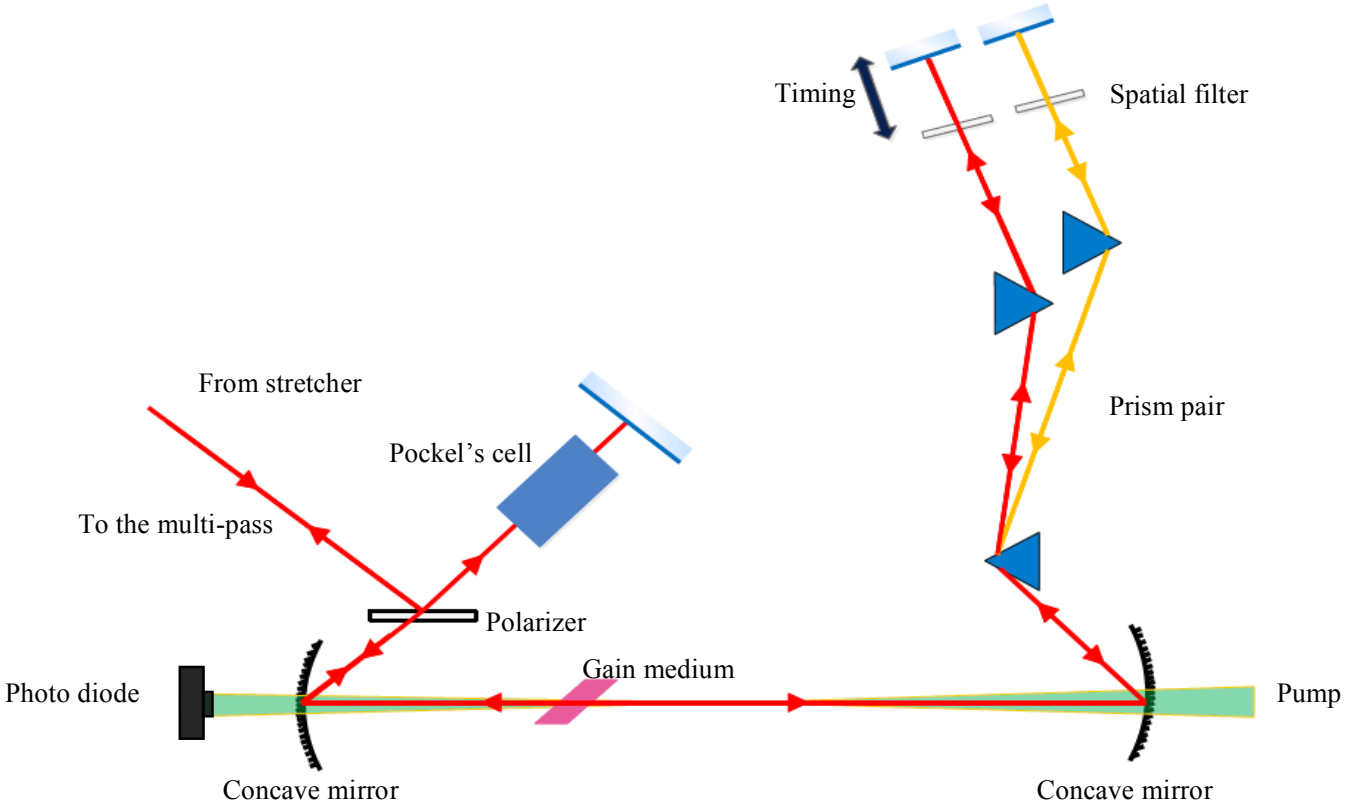

Figure 3.6: Dual wavelength Regenerative amplifier setup

One of the back mirrors in the cavity (usually the long wavelength's mirror), has been put on the translational stage. By changing the position of this back mirror, we can make sure that the two colors are together and the cavity has the same repetition rate for both of the colors.

The combination of the Pockel's cell and the polarizer work as the optical switch in our cavity [44]. This optical switch will make a periodic loss inside our cavity, and trap the seeding beam inside of it. The energy of the pump will be transferred to the trapped seeding pulse inside the cavity. Finally, the optical switch changes the loss of the system, and the pulse with the highest possible energy can be extracted from the cavity. Figure 3.7 shows the output spectrum of two the different colors, which is coming out from our Regen.

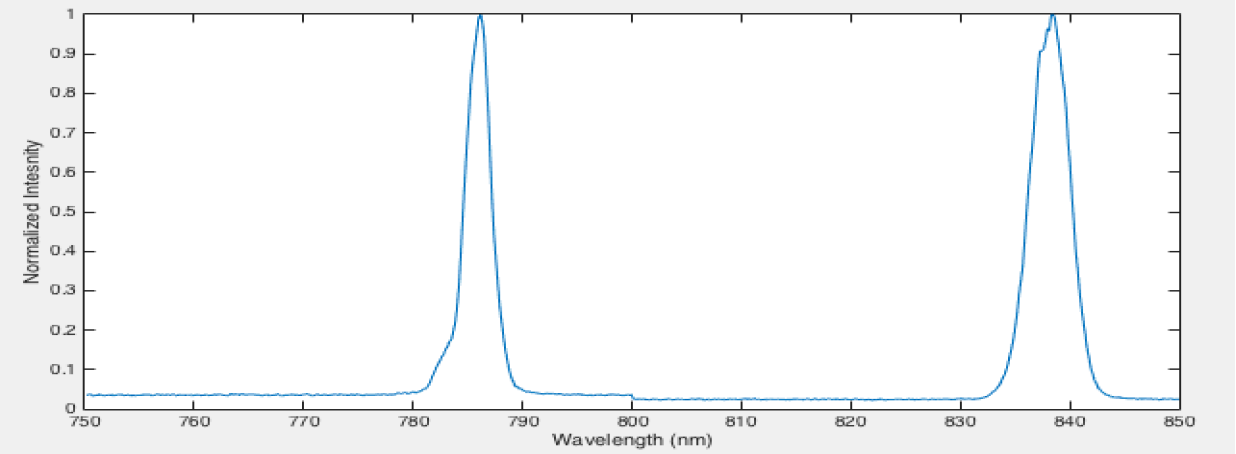

Figure 3.7: Measured spectrum from the Regenerative amplifier

Now, let us briefly explain how the combination of a polarizer and a Pockel's cell can works as an optical switch. We are using a commercial Medox Pockel's cell in our lab. The main advantage of a pocket cell is that by changing the voltage, we will have full control over the polarization of the laser beam. Inside of the Pockel's is a KDP crystal, which is a birefringence crystal. By applying a certain amount of voltage, the ordinary (O) and extraordinary (e) refractive index of this crystal will be changed. Then, this crystal can act as a half wave plate or a quarter wave plate. The seeding beam, which is coming from the stretcher, has the S polarization. The seeding beam will be reflected from the polarizer (Brewster effect), and it will go through Pockel's cell. The Pockel's cell initially is off, which works as a quarter wave plate. Then, the seeding beam will have a circular polarization. After the Pockel's cell, it will be reflected from the back mirror and will pass through the Pockel's cell one more time. Then finally the seeding beam will become P

polarized. The seeding beam will pass through the polarizer and enter the cavity. When the pulse enters the cavity, the voltage on the pocket cell will be changed, and the Pockel's cell will become to a half-wave plate. It means that the P polarized seeding beam will be trapped and oscillate inside the cavity. The following picture shows how the energy of the seeding pulse inside a regenerative amplifier will be changed as a function of the round trip. Frantz Nodvik equation for the gain can explain the behavior of figure 3.8 [45].

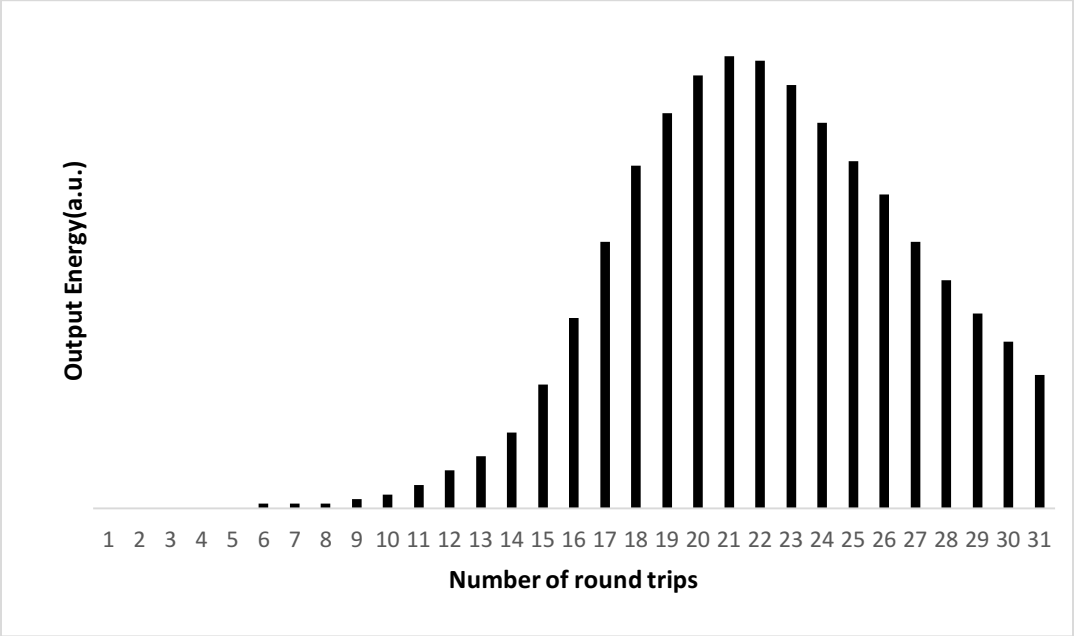

Figure 3.8: Output energy of the Regenerative amplifier as a function of the round trip

As we can see from figure 3.7, the energy of the amplified pulse will initially increase and finally decrease. To have an excellent amplification, the optical switch should be opened in the optimum case, and the pulse should be extracted with maximum energy. To have this scenario, the voltage of the Pockel's cell will be changed again, and will become a half wave-plate. In this case, the trapped amplified pulse will be extracted from the Regen cavity because the polarization will be changed again to the' S' state, and will be reflected from the polarizer.

The performance of the Pockel's cell is a crucial part of our setup. We need to monitor the performance, and try to avoid having amplified spontaneous emission (ASE). To monitor the overall performance of the Regen, we use a fast photodiode behind one of the concave mirrors to look at the small leakage. To have an excellent seeded and amplified pulse, we need to have sharp

spikes which represent the seeded pulse, and the background represents the ASE. Figure 3.9 shows the signal of a fast photo diode in two different cases of having a good or bad seeding.

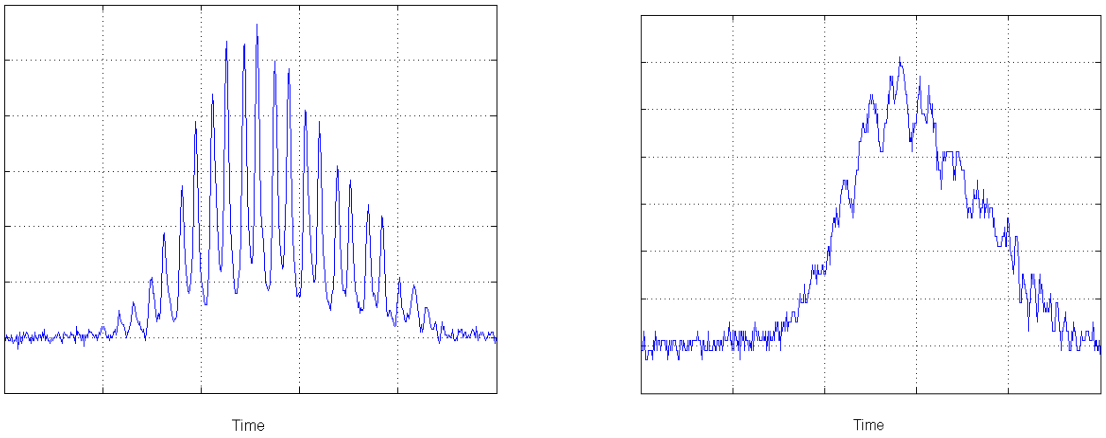

a) b)

Figure 3.9: Signal of fast photo diode in two different cases:
a) Regenerative amplifier has a good seeding
b) Regenerative amplifier has a bad seeding
adapted from [46]

3.1.4 Multi-pass Amplifier

In the designing of an amplifier, two different factor should be considered. The first one is the gain, and the second one is the energy extraction. It is not impossible to have a good gain and a proper energy extraction at the same time in only one stage amplification. It is always a trade-off. To solve this problem usually multistage amplification system is needed. Figure 3.10 shows how the amplification work.[15] [47]

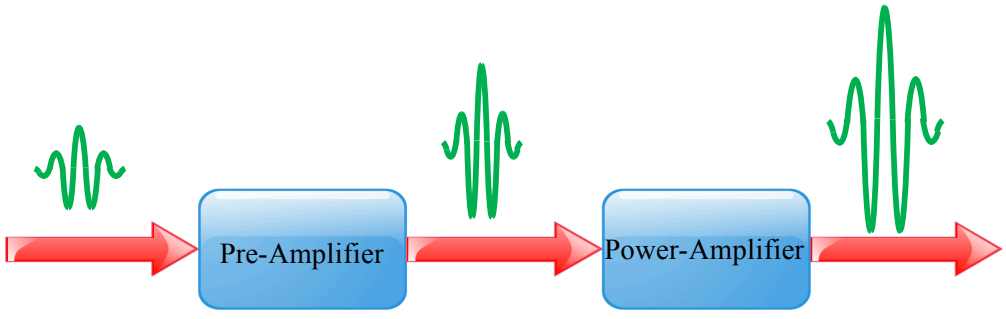

Figure 3.10: Multi-stage amplification system

The first stage, which is pre-amplification stage will provide a good gain to the seeding pulse, and the second stage will boost the energy of the pulse. As we have mentioned before, we use a regenerative amplifier as a pre-amplification system which provides an excellent gain for our two colors. After that, we use a multi-pass amplification system as the power amplifier, which boosts the energy of each pulse to 1.5 mJ. The multi-pass amplifier and Regenerative amplifier are working very similar to each other.

In the multi-pass amplifier, a few mirrors have been used to let the beam pass through the crystal with different angles, and the designing issues limit the number of the passes. It can be designed for 3, 4, or even 5 passes through the crystal.

In our setup, we use a multi-pass amplifier, which is designed to boost the energy 10 times higher. The pulses will pass through the Ti: Sapphire crystal 5 times. Moreover, the crystal will be pumped by the Nd: Yag laser from two sides to increase the energy extraction and to avoid damaging the crystal. Figure 3.11 shows the design of multi-pass amplifier with three-pass. (However, in our lab, we use a 5 pass multi-pass, which is hard to draw).

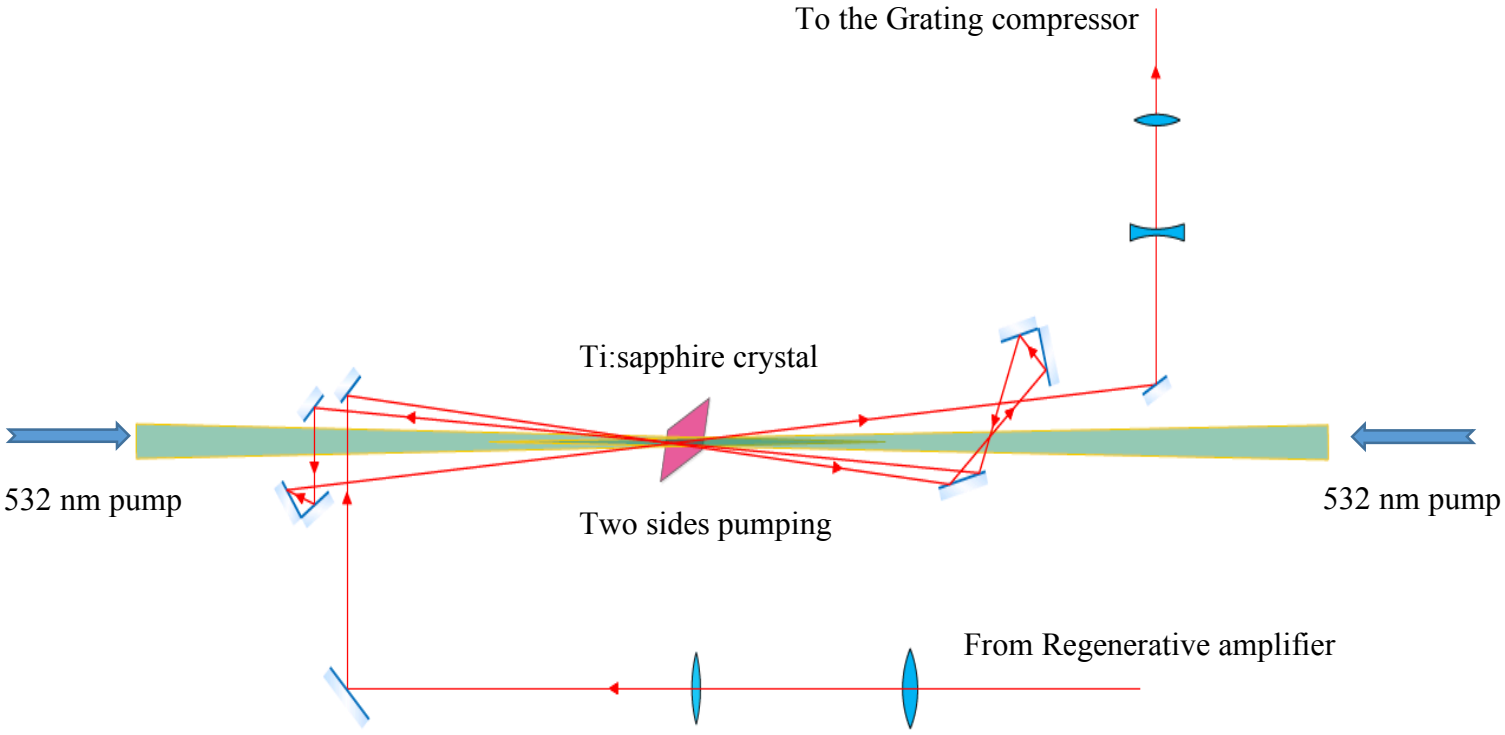

Figure 3.11: The Multi-pass amplifier setup

3.1.5 Dual Wavelength Pulse Compressor

The final stage of any CPA system is the compressor. Usually, the grating pair compressors are being used in compression systems because they provide a considerable amount of negative dispersion, which is really hard to get by other techniques like prism compressors. To reach the maximum compression, Fourier transform limit pulse, the total second order dispersion of the system should be zero. It means that:

$$\frac{\partial^2\phi}{\partial\omega^2}_{Stretcher} + \frac{\partial^2\phi}{\partial\omega^2}_{Material} + \frac{\partial^2\phi}{\partial\omega^2}_{Compressor} = 0 \tag{3.1}$$

Usually, the material and the and pulse stretcher will provide normal dispersion (Positive GDD). Then, the pulse compressor should provide anomalous dispersion (negative GDD). By having a perfect match between the normal and anomalous dispersion, it is possible to compress the pulse to the its transform limit.

In our experiment, we are using a dual wavelength pulse compression system to compress two different colors after being amplified by the multi-pass amplifier. In our setup, we have three different gratings. The first grating is the same for the two different colors. After the first grating, the two colors will be dispersed and separated. Because the frequency spacing between the colors is too much, it is not possible to use only one back grating. Then, two back gratings will be used to compress the colors separately. The distance between the gratings will determine the total negative dispersion of the compressor. In our setup, this distance is around 300cm. After the back gratings, we have the roof mirrors, which will send back two different colors to the grating pair, and finally, the beam will be directed to the hollow fiber assembly.

To avoid self-phase modulation, we leave a linear chirp on the each of the pumps. This can be easily done by placing the gratings in front of the optimum place. One of the back mirrors in the Grating compressor is placed on a portable stage, which will enable us to control the delay between the colors, and change the instantaneous frequency separation between the two chirped pumps. Figure 3.12 shows the experimental setup that we are using in our lab.

Also, it is critical to making sure that our compressor does not provides any spatial chirp. In order to verify it, we can move the spectrometer after the compressor to make sure that the output spectrum of the compressor is not a function of the position of the spectrometer.

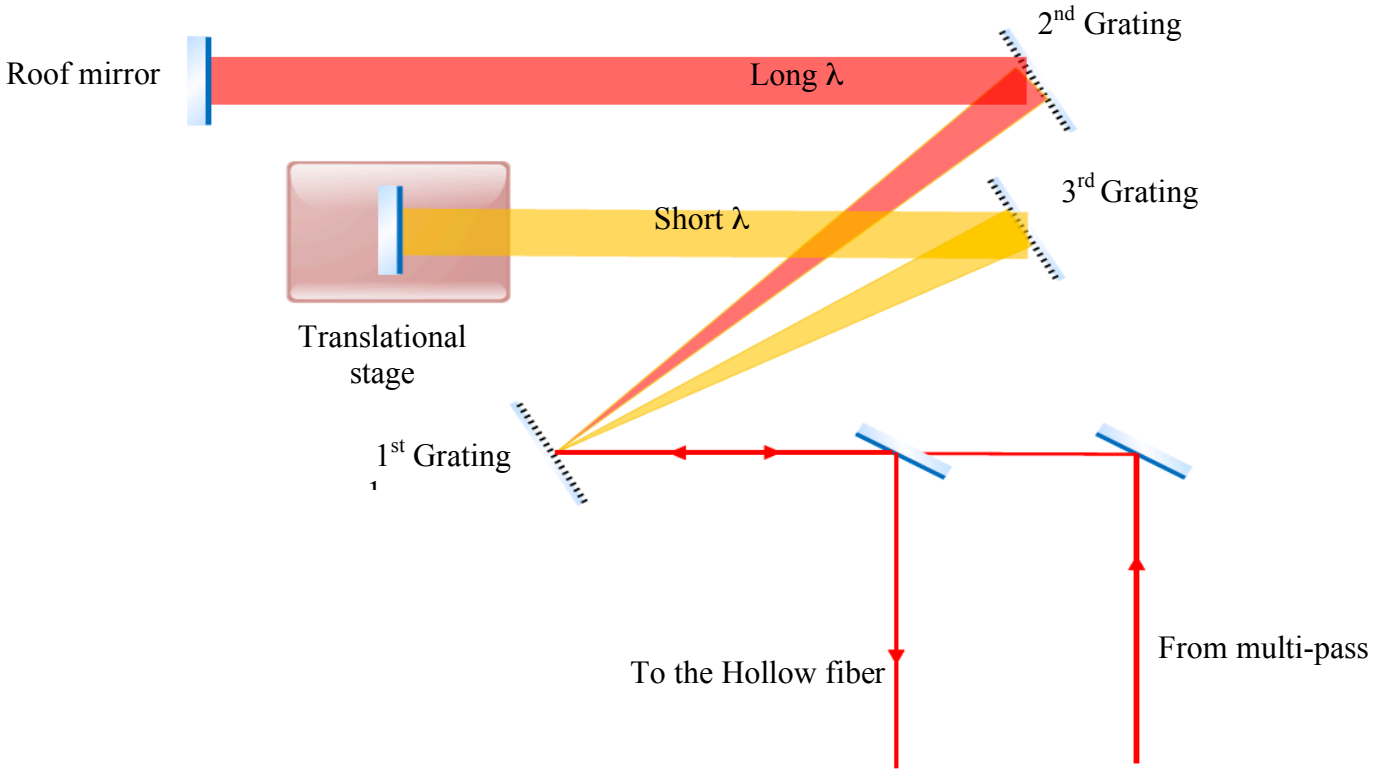

Figure 3.12: Dual wavelength grating compressor

3.1.6 Hollow Fiber Assembly

Nonlinear light-matter interactions need high and enough laser intensity. Focusing the laser beam by a lens is one of the easiest ways to achieve maximum possible intensity. However, in this case, the interaction length is limited to the Rayleigh length. After the Rayleigh length due to the diffraction, the intensity will significantly decrease, and the efficiency of nonlinear interaction will be decreased. Hollow core fibers are a good solution to increase the interaction length in a nonlinear experiment. The laser pulses will be directed inside of an optical fiber, and the final efficiency of the nonlinear interaction will be increased significantly [48] [49].

In our experiment, we are using a 0.5-meter-long hollow core fiber. The inner diameter of the fiber is 150 µm. Before the fiber, we use a focusing lens to focus and direct two different pumps in the optical fiber. After the fiber, we also use another lens to collimate the beam. Our fiber is placed in a sealed chamber which is filled with SF_6 gas. The chambers are placed on two X-Y translational stages to give us a good control of the position of the chamber. This translational stage will be

used to align the chamber, and to make sure that the beam is passing through the fiber with the maximum efficiency. We also use a CCD camera after the fiber to look at the profile of the beams. This CCD camera helps us to make sure that we have the maximum efficiency, also we can make sure that the pulses have the same cross-section, which means they are spatially overlapped. In our experiments, the pressure of the chamber was set at 10 psi.

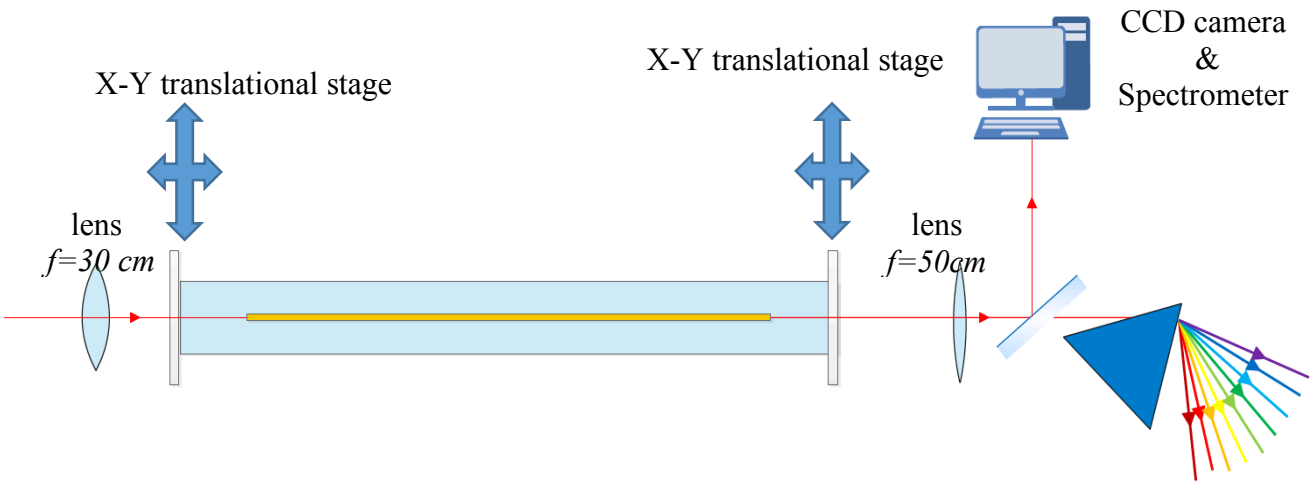

Figure 3.13: Hollow core fiber setup filled with SF_6 gas

3.2 Single-shot Autocorrelation:

In our experiment, we are using a single-shot autocorrelation system to measure the temporal duration of the pulses [50]. We have chosen this technique because the repetition rate of our laser is very low (10HZ). The single-shot autocorrelation gives us this opportunity to look at the autocorrelation trace of a single pulse, and use it to calculate the pulse duration.

In a single-shot autocorrelation, we are mapping the delay and the temporal information of a pulse into the position. This can be done by spatially overlapping two pulses in a nonlinear medium such as BBO crystal. Figure 3.14 shows the experimental setup for this technique. The setup and alignment for our autocorrelation can be a little bit tricky and need special care. The low repetition rate of the laser causes the pulses to be very far away from each. After the beam splitter, we make two copies from a pulse. These two copies should meet each other at the same time in the BBO crystal, then the length of the two arms should be the same. We are using a cylindrical lens in our system before the BBO crystal. This lens focuses the pulse and its copy to a line, and after that, the beams have an overlap in the BBO crystal.

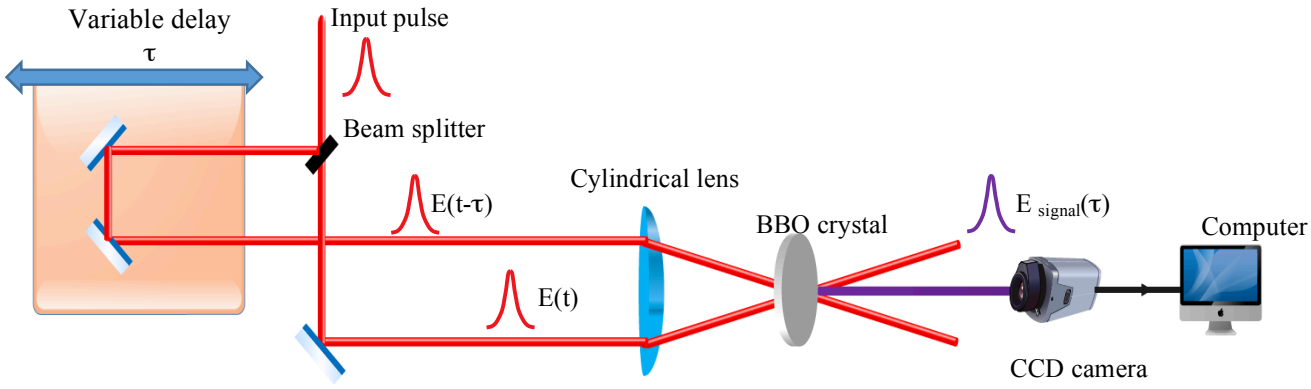

Figure 3.14: Single-shot non-collinear autocorrelation setup.

After the BBO crystal, we use a CCD camera to look at the autocorrelation trace. The width of the autocorrelation trace will be a function of the pulse duration. The CCD camera is connected to a computer, which can record the intensity of every single pixel. After the integrating over the screen, we can generate the autocorrelation curve. Then, we can calculate the full-width at half maximum(FWHM) of the autocorrelation curve as a function of the pixel. To extract the temporal information from the curve, we need to find the calibration factor. In the other word, we need to

know what is the meaning of each pixel on the CCD camera, and each pixel is representing how many femtoseconds. To do this, we use the translational stage. By moving the translational stage, we give a delay to one of the pulses. This will cause the whole autocorrelation trace to move on the screen. Then, we can record how much a certain delay moves the peak pixel. This technique will lead to finding the calibration factor which is around 18 fs/pixel for our setup.

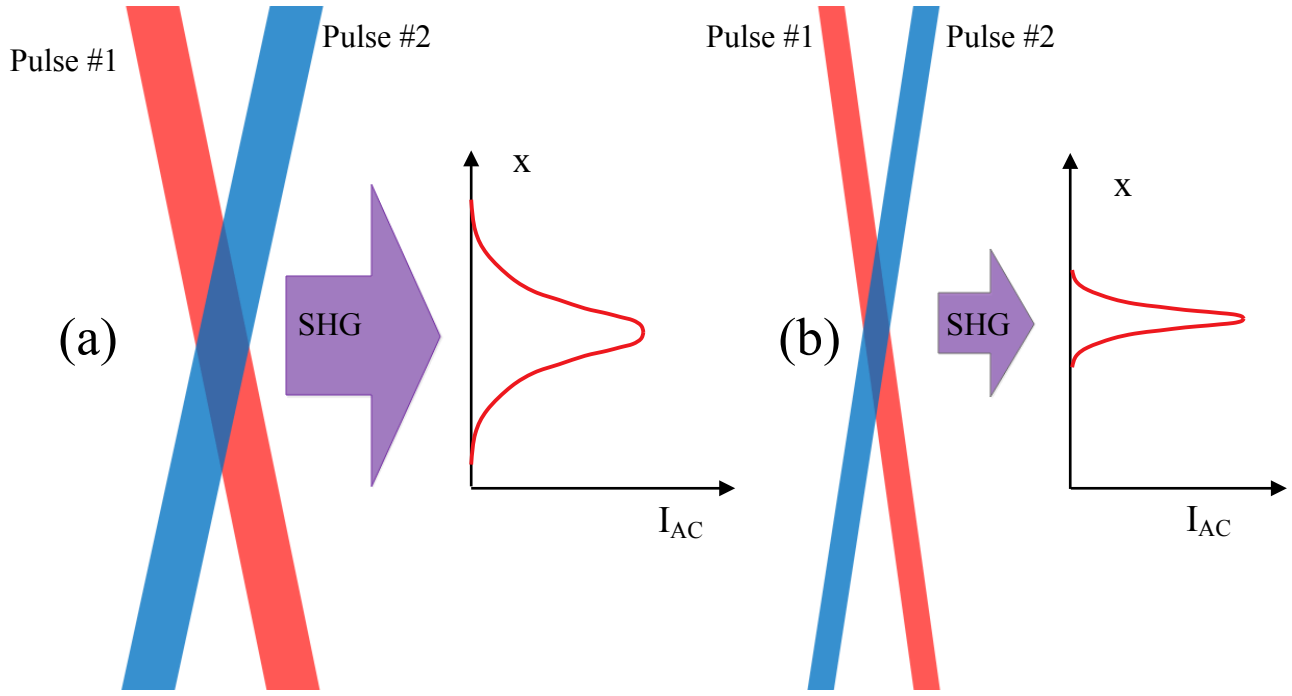

Figure 3.15: mapping the temporal profile of the pulse into position.
(a) and (b) shows that the spatial width of the second harmonic signal is a function of the duration of pulse.

Figure 3.16 Sample Autocorrelation trace recorded by the CCD camera

3.3 Pulse Compression System:

The final stage of this work is compression of the first anti-Stokes order. The short-term goal of this compression is to study the behavior of the red-shifted shoulder in MRG, and how this extra bandwidth will affect our pulse compression. The long-term goal of this compression is to compress different orders with red-shifted shoulders and adding them coherently together to generate a single femtosecond pulse. We are using a prism pair pulse compression system in our lab to achieve our goal. Our prisms are made of SF10, which is very dispersive glass and appropriate choice for dispersion compensation.

After the hollow fiber, we are using three lenses to make sure that the beam is collimated and have an excellent Gaussian profile. If the size of the beam is small, it is hard to get the autocorrelation trace and measure the pulse duration. Moreover, if it is very large the intensity will decrease and also the autocorrelation does not have good quality. So by trying the different lens with different focal points, we can make sure we have a beam with the best profile.

After the collimation system, our beam will pass the first prism. After the first prism different orders will be separated. We can use an adjustable slit only to let the orders that we want to pass and go to the compressor. Figure 3.17 shows different separated orders after the first dispersive prism.

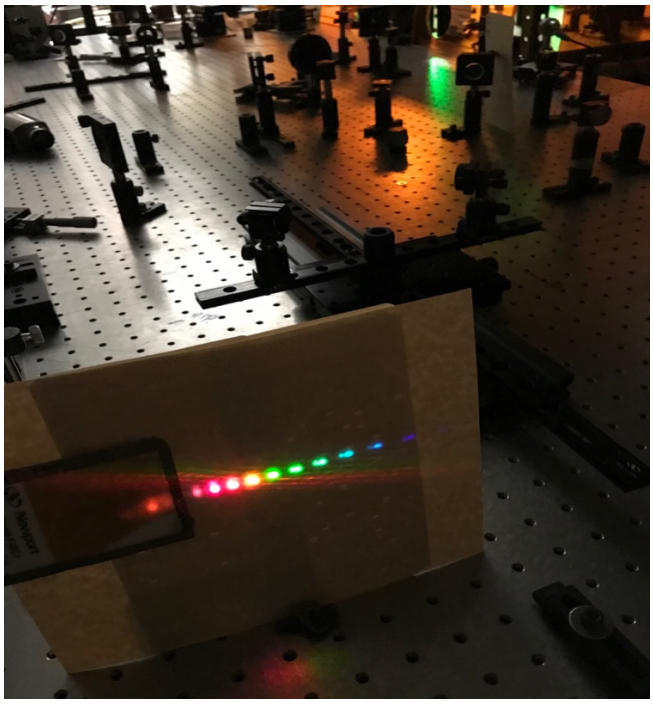

Figure 3.17: The MRG rainbow spread from near-IR to UV

Between the two prisms, we have a translational stage, which enables us to change the distance between the two prisms. By changing the distance, we have good control over negative GDD of the system. Also, both of our prisms are placed on the translational stages. They are carefully aligned with the minimum deviation angle which enables us to move the prisms perpendicular to the beam path and avoid any miss alignment of the beam. The movement of the prisms will enable us to have control over the positive GDD of the system. Then by changing the distance between the prisms and moving vertical movement of the prisms, we can have excellent control over the positive and negative GDD of our compression system which makes the tuning and compression very easy.

To have maximum compression, we need to avoid spatial chirp of the pulse after our compressor. The spectrometer can quickly check this. We can place the spectrometer after the compressor and before the autocorrelation to check whether we have spatial chirp or not. If the spectrometer shows that after the compressor the frequency is a function of the space, this means spatial chirp exists and has an impact on the final pulse duration, so we need to go back and recheck the alignment of the prisms. The following picture shows the experimental setup for our pulse compression system.

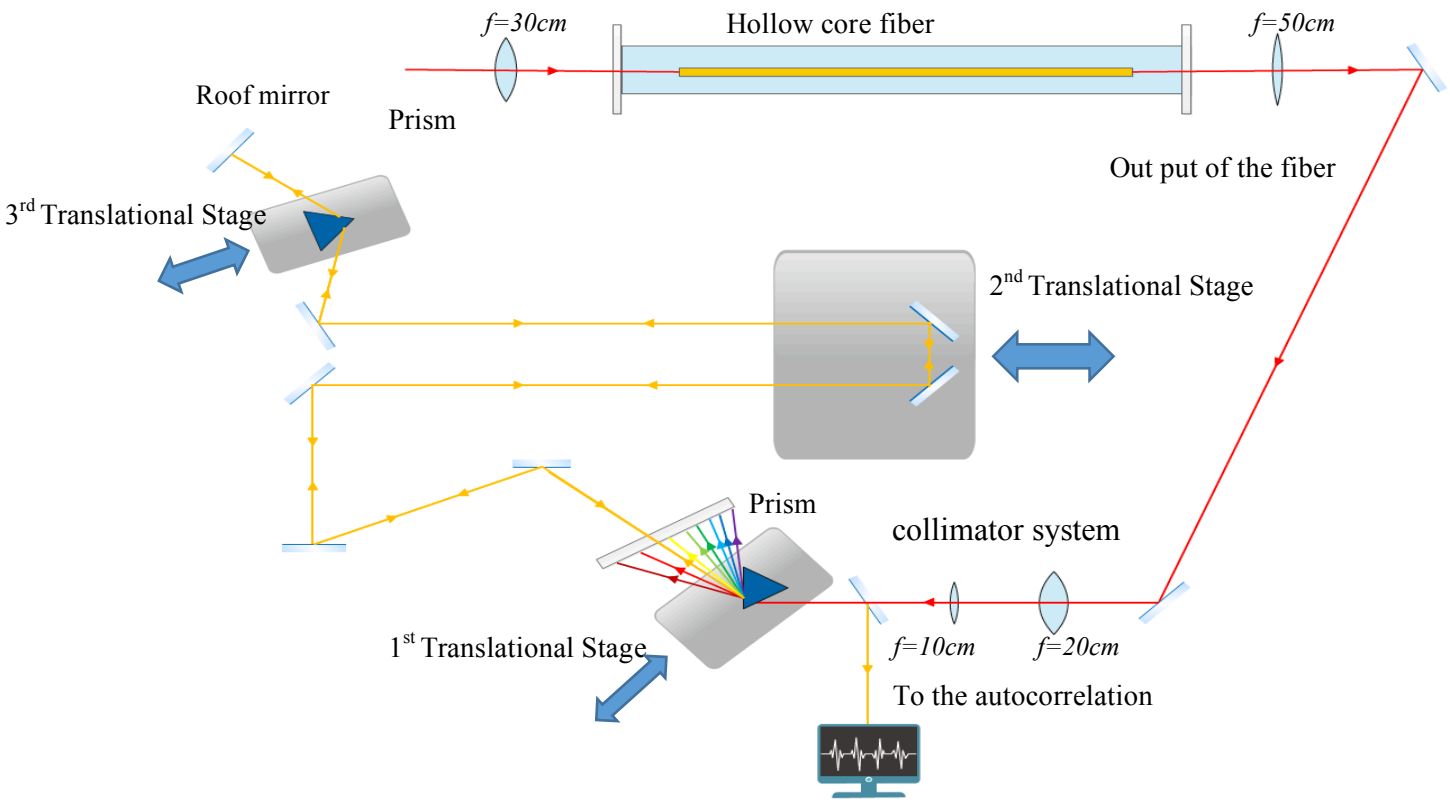

Figure 3.18: Pulse compression setup

Chapter 4

Experimental Results & Discussion

In this chapter, we will present our experimental results and discuss these findings. The primary goal of this chapter is to get a better understanding of the red-shifting process in MRG. We are going to investigate how this extra frequency bandwidth affects the compression of first anti-Stokes order. Can this extra bandwidth help us to have better pulse compression? Alternatively, if not, what is the main obstacle for compressing the Raman order, and how this bandwidth should be used.

As we have mentioned before, we are using two chirped pump pulse to study MRG for two reasons. The first one is that by using two chirped pulse, we can avoid SPM. The SPM will broaden the spectrum of each pump pulse, and this will significantly decrease the efficiency of MRG. The other reason is that the two chirped pump pulse will enable us to change the instantaneous frequency between the two pumps. We can tune the frequency separation between the pulses, which gives us a great tool to study the red-shifting of different Raman orders. By physically moving one of the back mirrors in our dual-wavelength pulse compressor, we are changing the delay between the two pulses. This will eventually lead to the change of the frequency separation between the pumps.

4.1 Spectral Measurement of Red-shifted Spectrum

As we have mentioned before, the long color is centered at 837 nm, and the short color is centered at 786 nm. Both of them have the same bandwidth of 3 nm. The pulse duration of the long color is set to 800fs, and the pulse duration of the other color is set to 900 fs. This difference in pulse duration is because we want to have the same chirp rate for both of the pumps. With the mentioned pulse durations and wavelengths, the two pumps will have the same chirp rate of 1.6 THz/ps. The frequency difference between the center wavelength of the two pumps is around 50 nm, which corresponds to the first Raman state of the SF_6 gas. The instantaneous frequency separation between the two pumps can be written as follows:

$$\Delta f_{sep} = \alpha \Delta t + 23.25\ THz \tag{4.1}$$

where the α is the chirp rate of the pumps (1.6 THz/ps), Δt is the delay between the pumps, and 23.25 THz is Raman frequency of SF_6.

If the Δt be zero the two pumps are perfectly overlapping in time, which cause to have the maximum efficiency in the MRG process. In this section, we change the delay between the pumps, which change the frequency separation between the pumps. By changing the frequency separation, we record the first anti-Stokes order spectrum by OSA. This helps us to look at the evolution of red-shifted shoulder as the function of frequency separation between the pumps. The following figures shows the dependence of red-shifter shoulder of first Raman order for different frequency separations:

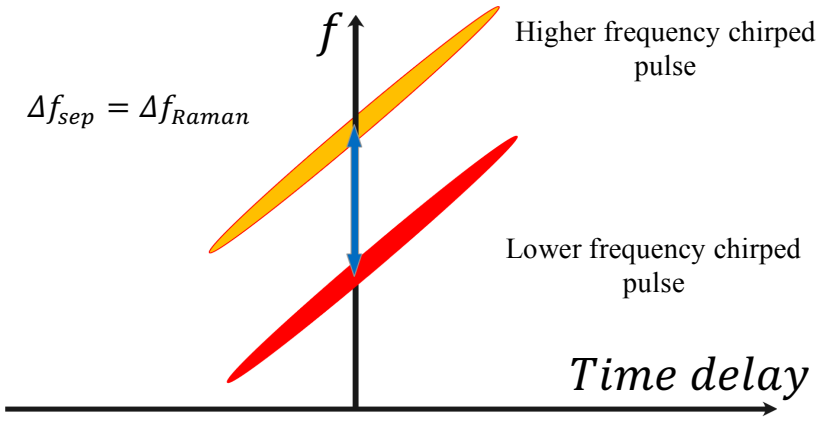

Figure 4.1: Description of two chirp pump pulse with following conditions:
$\Delta f_{sep} = 23.25\ THZ$
$\Delta t_{delay} = 0$

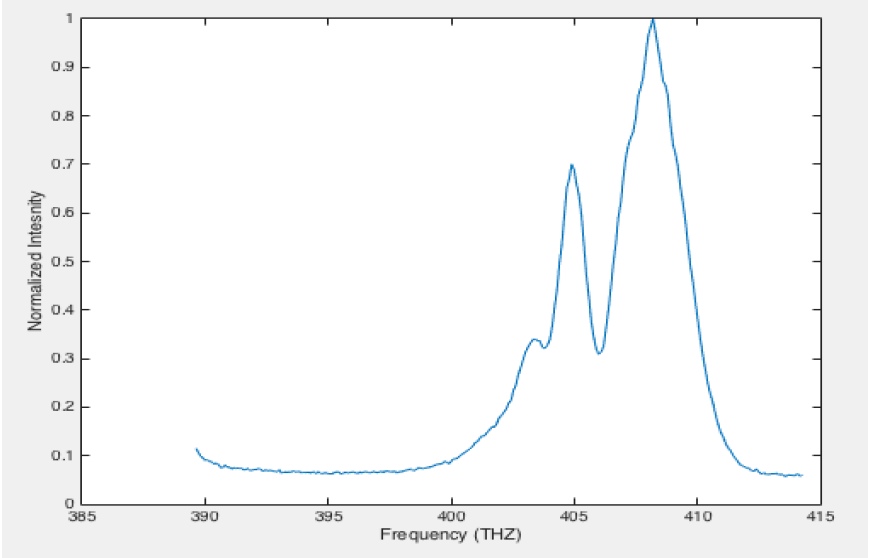

Figure 4.2: First anti-Stokes order spectrum with a red-shifted shoulder

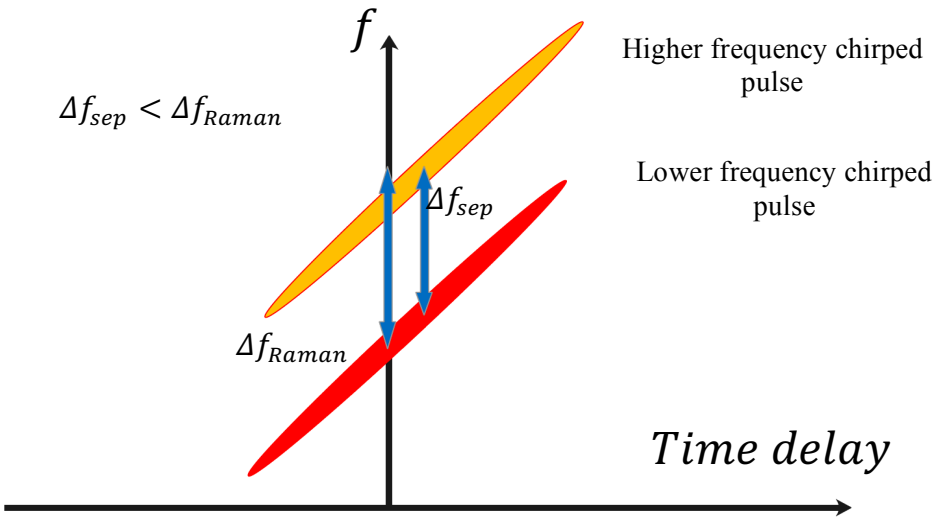

Figure 4.3: Description of two chirp pump pulse with following conditions:
$\Delta f_{Sep} = 22.61THZ$
$\Delta t_{delay} = +400fs$

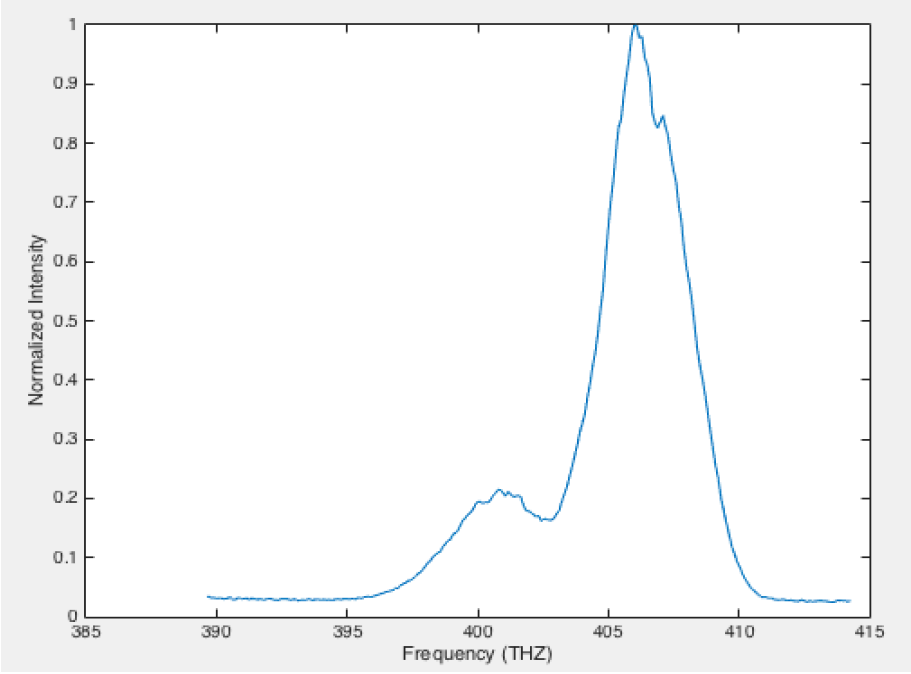

Figure 4.4: First anti-Stokes order spectrum with a red-shifted shoulder

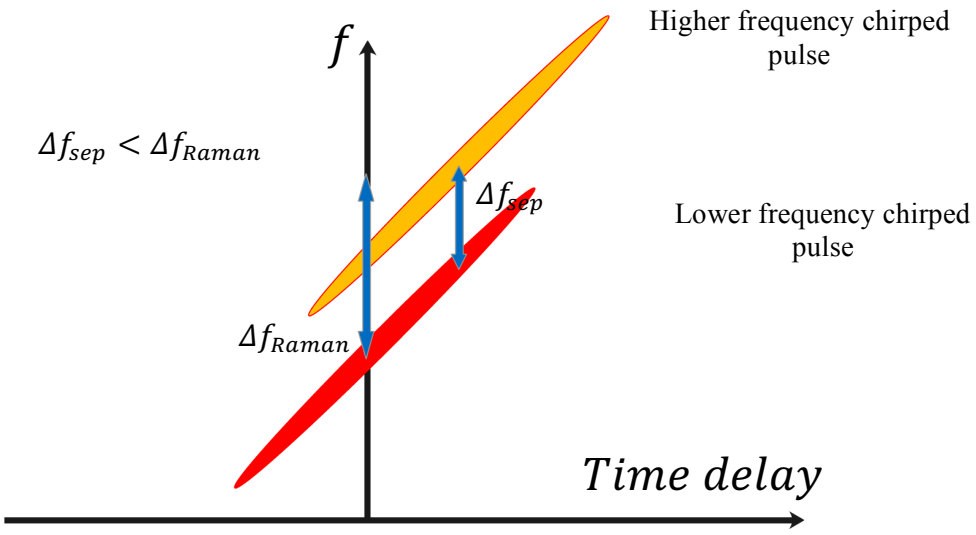

Figure 4.5: Description of two chirp pump pulse with following conditions:
$\Delta f_{sep} = 21.97\ THZ$
$\Delta t_{delay} = +800fs$

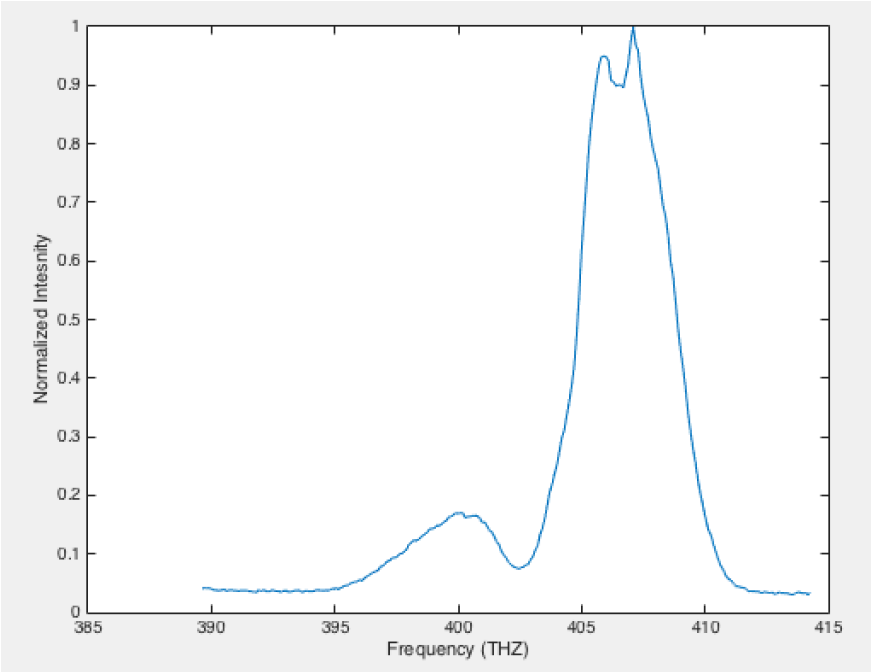

Figure 4.6: First anti-Stokes order spectrum with a red-shifted shoulder

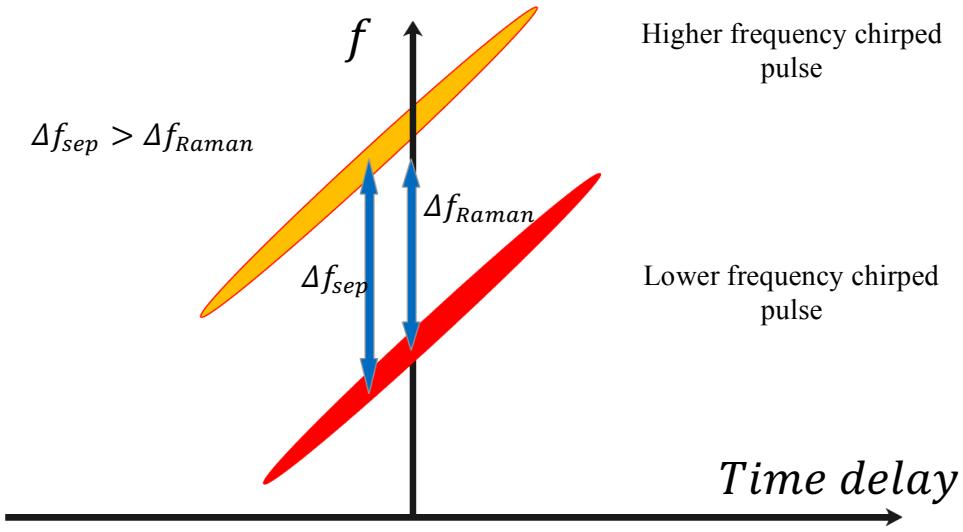

Figure 4.7: Description of two chirp pump pulse with following conditions:
$\Delta f_{sep} = 23.89\ THZ$
$\Delta t_{delay} = -400fs$

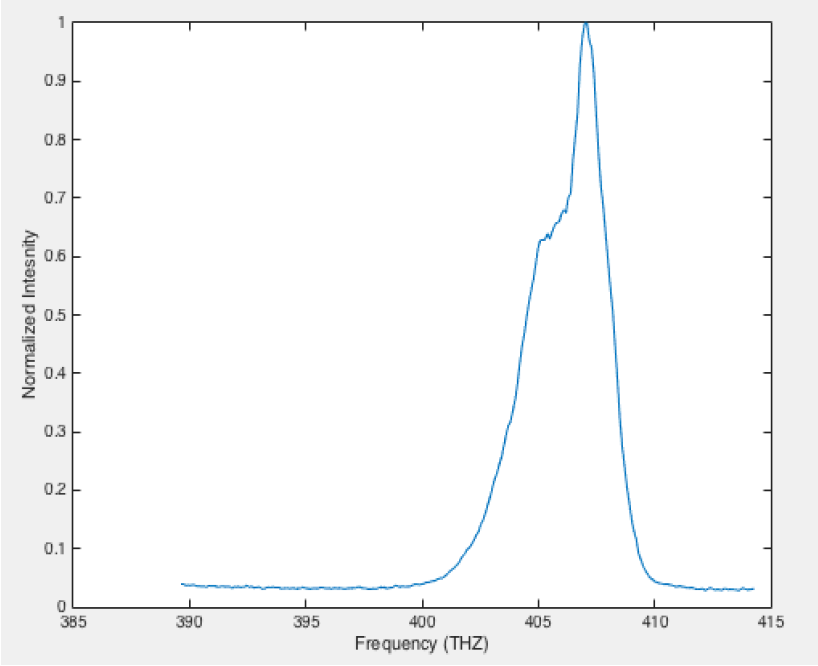

Figure 4.8: First anti-Stokes order spectrum with a red-shifted shoulder

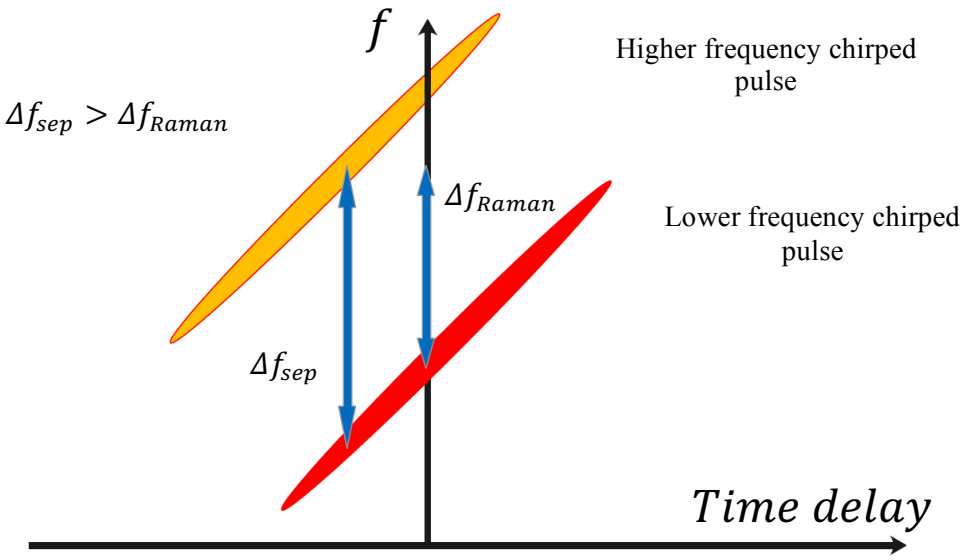

Figure 4.9: Description of two chirp pump pulse with following conditions:
$\Delta f_{sep} = 24.53\ THZ$
$\Delta t_{delay} = -800 fs$

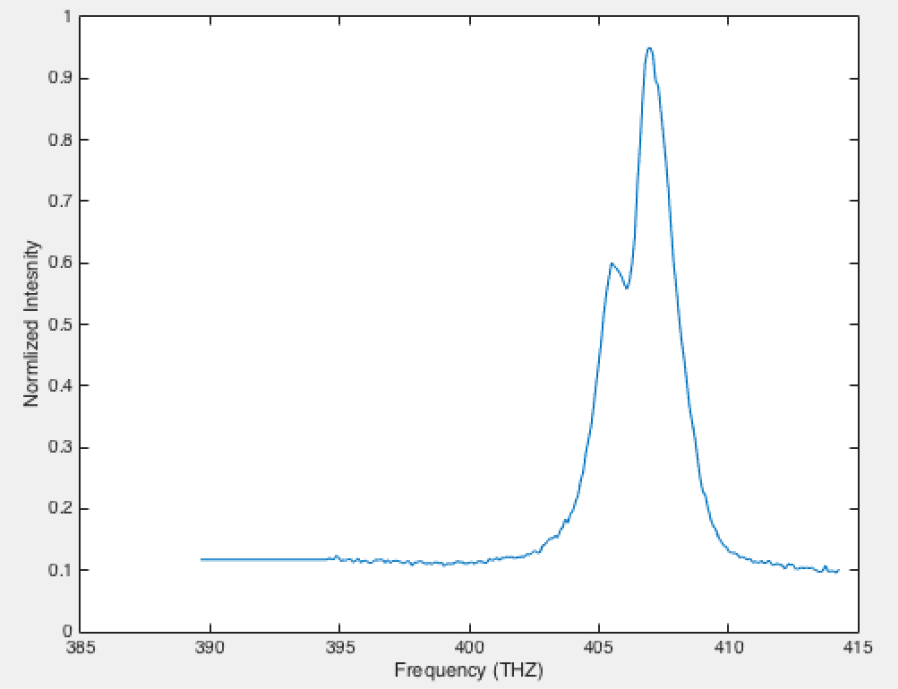

Figure 4.10: First anti-Stokes order spectrum with a red-shifted shoulder

The previous figures show the specific spectrum of the first Raman order for different time delays. As we have mentioned before, this delay will change the frequency separation between the two pumps. Figure 4.11 shows the relation between the frequency separation and time delay:

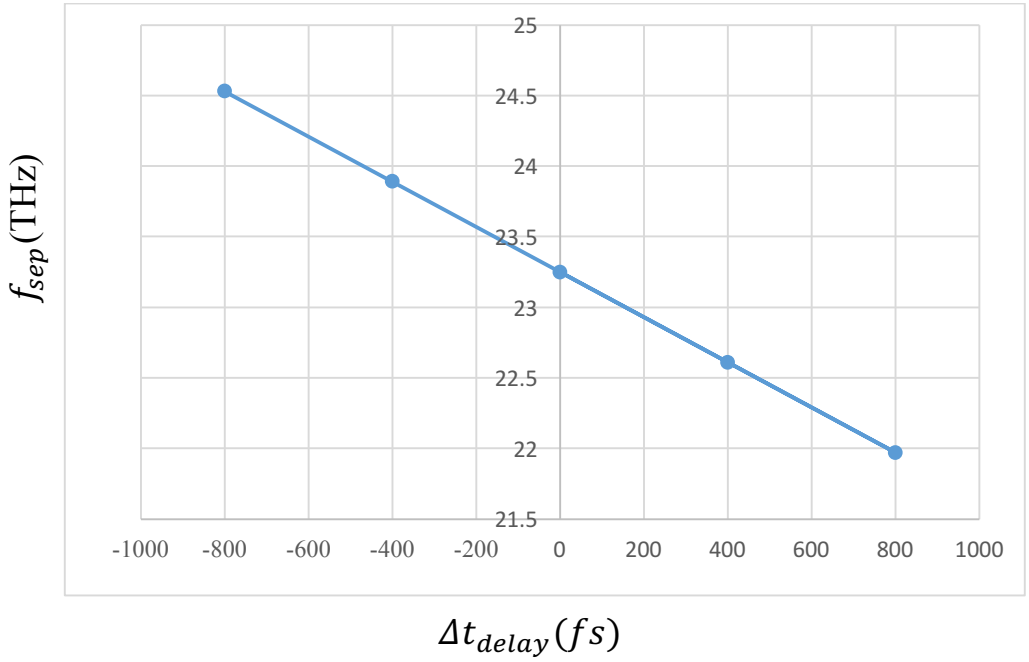

Figure 4.11: Instantaneous frequency separation of the pumps as a function of time delay

Now, we can look at frequency separation between the two peaks as function of the instantaneous frequency separation of the pumps. Figure 4.12 shows this dependence:

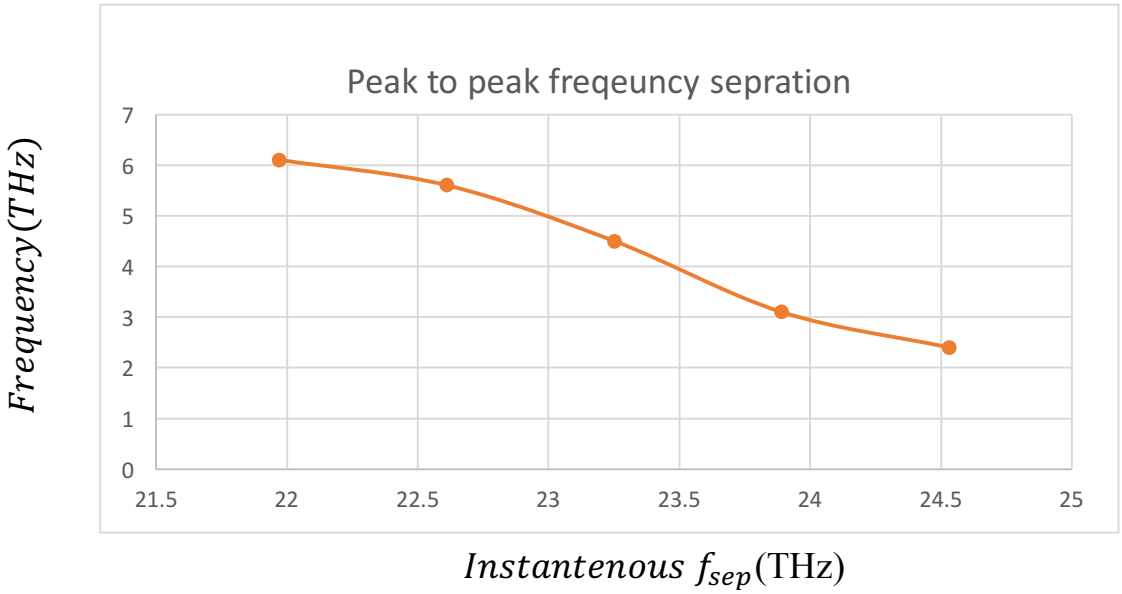

Figure 4.12: Frequency separation between the anti-Stoke order and red shifted shoulder as a function of instantaneous frequency separation

Our results show that the peak to peak frequency separation of the first anti-Stokes order and the red-shifted shoulder can be more than 6 THz if the instantaneous frequency separations are red tuned. In order to study about the red-shifted shoulder, we use our pulse compression system to compress the first anti-Stokes order with the maximum red-shifted shoulder, and we use our autocorrelation to record the results.

4.2 Pulse Compression of First Anti-Stokes Order

As we have mentioned before, the primary goal of our research is generation one femtosecond pulse through MRG. In our lab, we have used two chirped pumps to have the maximum efficiency and have the maximum number of the Raman orders, which provides us a broad spectrum. MRG process is a coherent process, which means all the Raman orders are highly correlated with the pumps. Then, all the orders are also positively chirped. In order to add all the orders coherently together, the phase of each order should be corrected and compressed. We are using our pulse compression system to do this task.

This section has two parts:

First, we try to compress the first Raman order in the absence of the red-shifted shoulder. By doing this, we will show that it is possible to correct the phase of the first Raman order and compress it to its Fourier transform limit. Finally, we try to compress the first Raman order in the presence of red-shifted shoulder to study more about the red-shifted shoulder. In the other word, we are interested to find how can we use this extra frequency bandwidth.

4.2.1 Compressing the First Anti-Stokes Order Without Presence of the Red-shifted Shoulder

In order to design a pulse compressor, we need to have the information about the bandwidth and the duration of the pulse, which is going to be compressed. Then, we can calculate how much GDD our compression system should provide. As we have mentioned before, we use a prism compressor to do the compression task. The final amount of GDD that our compression system can provide is a function of the separation between the prisms and the prism's material. Our pumps have the duration around 800 fs. Then, the first anti-Stokes order has also the same duration. The bandwidth

of the first anti-Stokes order without any red-shifted shoulder is around 3nm. This order is centered at 738nm.

By using equation 2.52 (Time-Bandwidth product for Transform-Limited Gaussian shape pulses), we can find the minimum pulse duration for the first Raman order is around 300 fs. Now, the stretched pulse duration is 800fs, and the shortest possible compressed pulse is 300fs. By having this information, we can calculate how much negative GDD our compressor should provide. By using equation 2.40 we can calculate the needed amount of GDD for compression, which is around 80000fs^2.

To provide this amount of GDD, we use a prism pair made from SF10 glass. By using equation 2.50, the prism separation should be around 4m.

The following diagram, shows the duration of the compressed pulse for different prism separations:

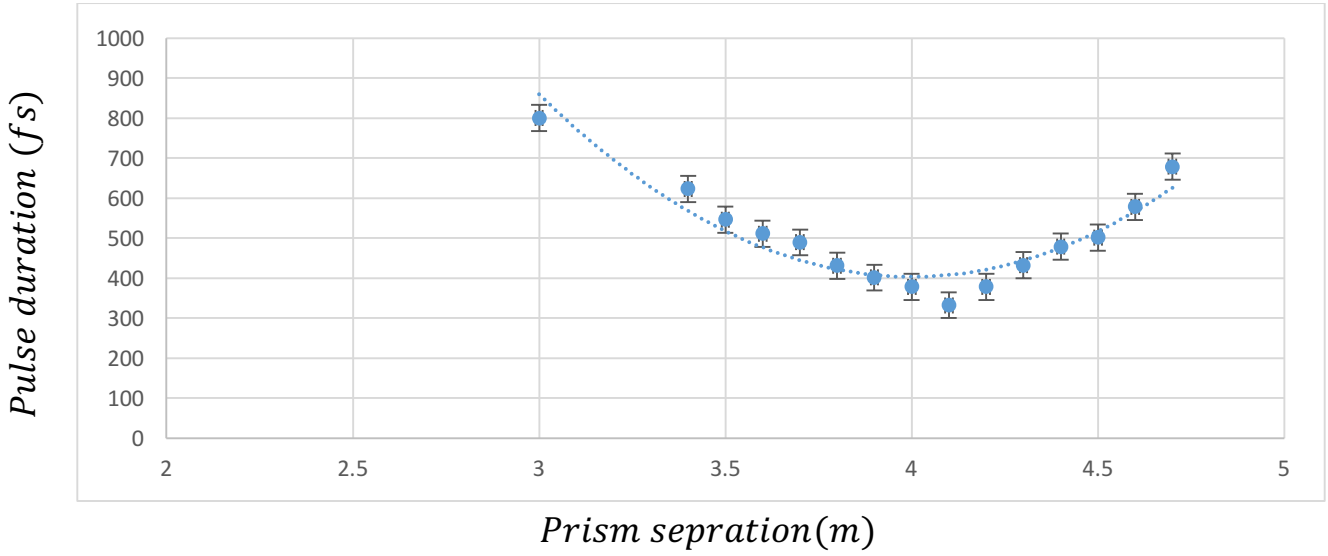

Figure 4.13: experimental results of the duration of the compressed pulse as a function distance between prisms

As we can see from figure 4.13, it is possible to compress the Raman order to near Fourier transform limit, which is excellent news. By doing this for the other orders, we can lock the phase of all of them, then add them together. This will promise to have a single femtosecond pulse with high peak power. Unfortunately, because of the limitation that we have in our lab, we could not compress more than one order at the same time. The main limitation is that the orders are far away from each other and it is not possible to use a single pulse compressor for all of them. Each of them needs to be compressed by a prisms pair and then adding all of them together.

4.2.2 Compressing the First Anti-Stokes Order with Presence of the Red-shifted Shoulder

The final step is to use the autocorrelation setup and the prism compressor to study the red-shifted shoulder's effect in the MRG process. Figure 4.6, shows the maximum possible red-shifted shoulder. It is clear for us that the red-shifting of the Raman order can double the frequency bandwidth of the first anti-Stokes order.

Then, we direct the first Raman order to our prism compressor. After the compressor, we use our single-shot autocorrelation setup to look at the compressed Raman order, but the results were surprising.

Surprisingly, we have seen that our autocorrelation trace has three separate peaks. This three distinct peak reveal an exciting fact about the red-shifted shoulder in the MRG process. This fact is that in the presence of the red-shifted shoulder, the output of the MRG contains two separate pulses, which is probably coming from two different processes. Figure 4.14 shows the autocorrelation trace that we have recorded in the lab.

Figure 4.14: three peak autocorrelation recorded by CCD camera

In order to explain why three peaks in the autocorrelation trace mean two separate pulses, we need to look at the figure 4.15, which beautifully explains this process. If we have two different pulses, blue and red in the figure 4.15, with a temporal delay between them, there will be four different intersections between the pulses. In these four intersections, the SHG will create four pulses. Two of the generated pulses are in the same line, then the output of the process has three separate peaks. These three peaks contain the temporal information of the two pulses, But the deconvolution process is not an easy task.

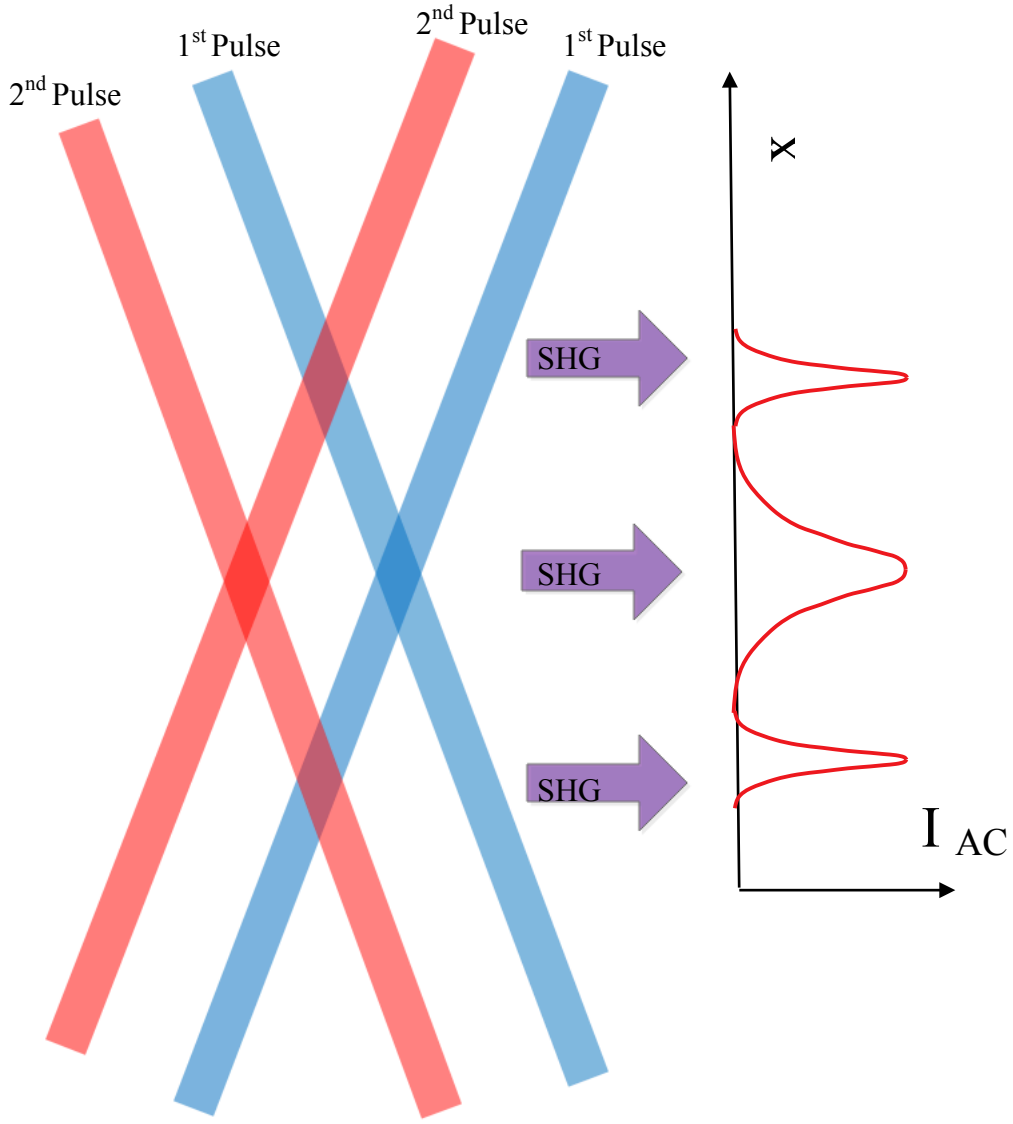

Figure 4.15: Single-shot double-pulse autocorrelation trace. Four different signal from the SHG process will make three separate peaks in the autocorrelation trace

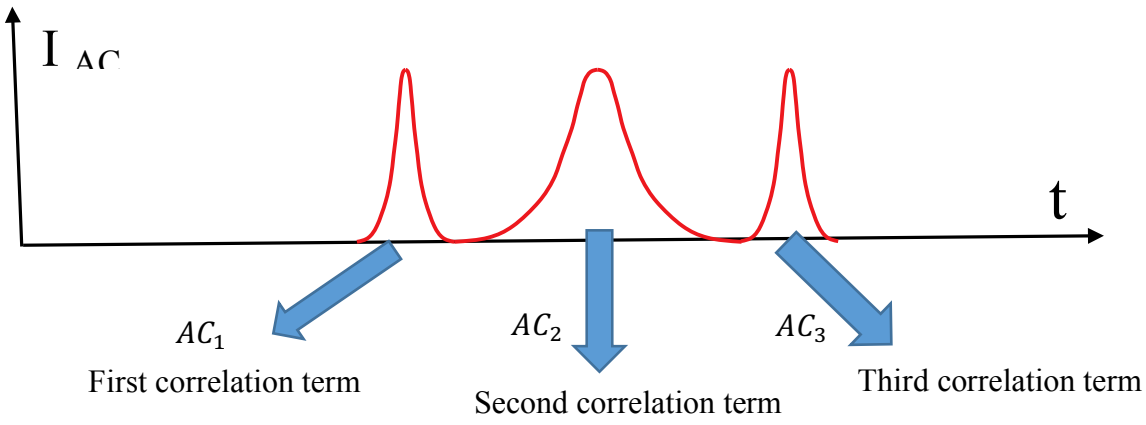

Figure 4.16: Each peak in the autocorrelation trace coming from a different correlating process

Then we can address each of the correlation function to an independent process, which are as follows:

$$AC_1 = \int_{-\infty}^{+\infty} I_{1st}\,(t) I_{2nd}(t-\tau)dt \tag{2.4}$$

$$AC_2 = \int_{-\infty}^{+\infty} I_{1st}\,(t) I_{1st}(t-\tau)dt + \int_{-\infty}^{+\infty} I_{2nd}\,(t) I_{2nd}(t-\tau)dt \tag{2.5}$$

$$AC_3 = \int_{-\infty}^{+\infty} I_{2nd}\,(t) I_{2nd}(t-\tau)dt \tag{2.6}$$

As we can see from the above figure, different peaks in our autocorrelation trace are coming from different functions. The first peak is coming from the cross-correlation of the first pulse and the second pulse. The second peak has two different terms: the first term is resulting from the autocorrelation of the first pulse and itself, and the second term is resulting from the autocorrelation

of the second pulse and its term. Finally, the third peak in our autocorrelation trace is resulting from the cross-correlation between the second pulse and the first pulse.

Now it is clear for us that in the presence of red-shifting process we have two distinct pulses, which one of them is coming from the Raman process and the other one is coming from another unknown process, which we call it red-shifted pulse

In order to get more information about the duration of the Raman and red-shifted pulse, we have used our autocorrelation and pulse compression setup to study these pulses. Our spectrometer shows that the maximum frequency separation between the pulse and red-shifted shoulder is around 7 THz. By using the compressor, we can get a little information about the spectral phase of the two pulses.

Figure 4.13 shows the duration of the pump pulse as the function of the separation between the prisms. We can also use figure 4.13 as a reference for the duration of the Raman order. Then we can measure the autocorrelation for different prism separations. We have got different autocorrelation curves for different prism separations. Then we can numerically guess that how much is the duration of the red-shifted pulse.

We have used different separation between the prisms and collected the data. The prisms separations are approximately 4m, 3.5m, and 3m. Figure 4.17, 4.19, and 4.21 shows the autorotation curves for different prism separations. Then we can reconstruct the pulses. Figure 4.18, 4.20, and 4.22 shows the calculated pulses. The cross-correlation of these pulses can approximately produce the experimental autocorrelation curves that we have got after the compression.

The results are surprising. The results show that the two pulses do not have the same spectral phase. By increasing the distance between the prisms, we are adding more negative dispersion this will compress the Raman order, and our results confirm that. Surprisingly, our constructed pulses show that the red-shifted pulse is not being compressed. By increasing the prisms separation, the red-shifted shoulder actually becomes broader. This is an exciting result because it shows that the Raman and red-shifted pulse does not have the same spectral phase (Assuming, the Raman pulse has the same chirp). The Raman pulse has the same chirp that the pumps have, but it seems that the red-shifted pulse does not have the same chirp at all.

First Autocorrelation Curve and Pulse Reconstruction: (Prism separation ~ 4m)

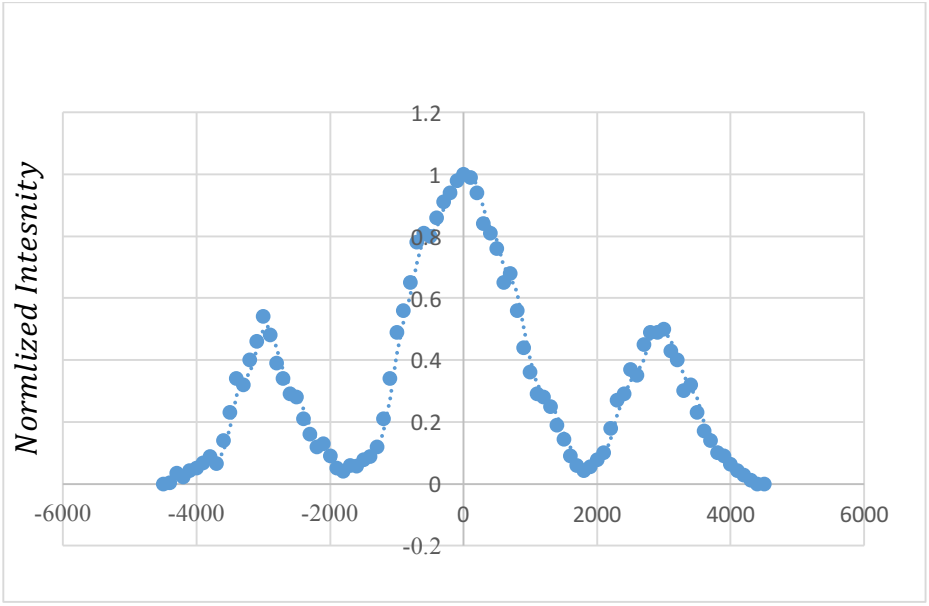

Figure 4.17: Experimental Autocorrelation curve of first anti-Stokes order in the presence of red-shifted shoulder

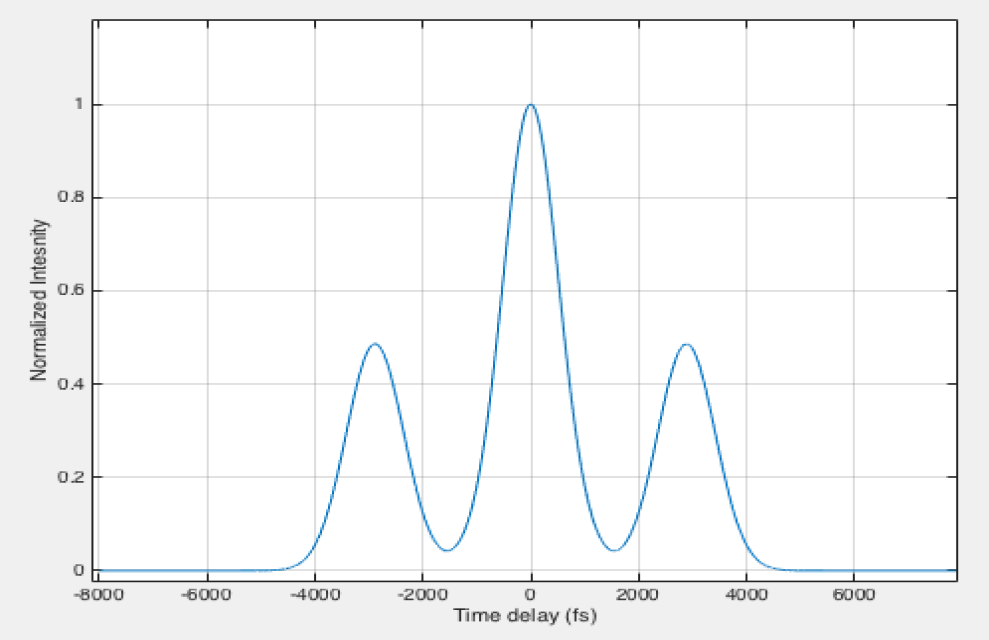

Figure 4.18: Simulated Autocorrelation curve of first anti-Stokes order in the presence of red-shifted shoulder

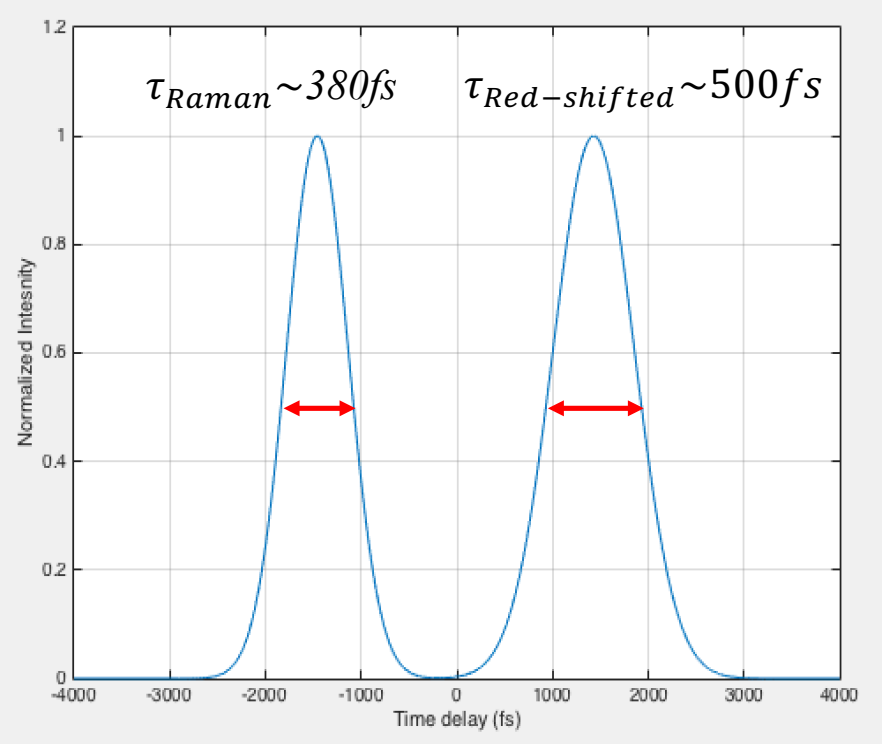

Figure 4.19: The two Gaussian pulses input, which will construct the 4.18 curve

Figure 4.17 shows the experimental result of the compressed pulse. We used the Gaussian pulses in figure 4.19 to construct the experimental result, which is presented in figure 4.18.

Our experimental autocorrelation curves show that the separation between the peaks is around 2.6ps. The duration of the Raman pulse is around 300 fs, and the duration of the red-shifting pulse is around 500fs.

Prims separation: 4 m

Duration of Raman Pulse: 380 fs

Duration of red-shifting pulse: 500 fs

Temporal delay between the pulses: 2600 fs

Second Autocorrelation Curve and Pulse Reconstruction: (Prism separation ~ 3.5m)

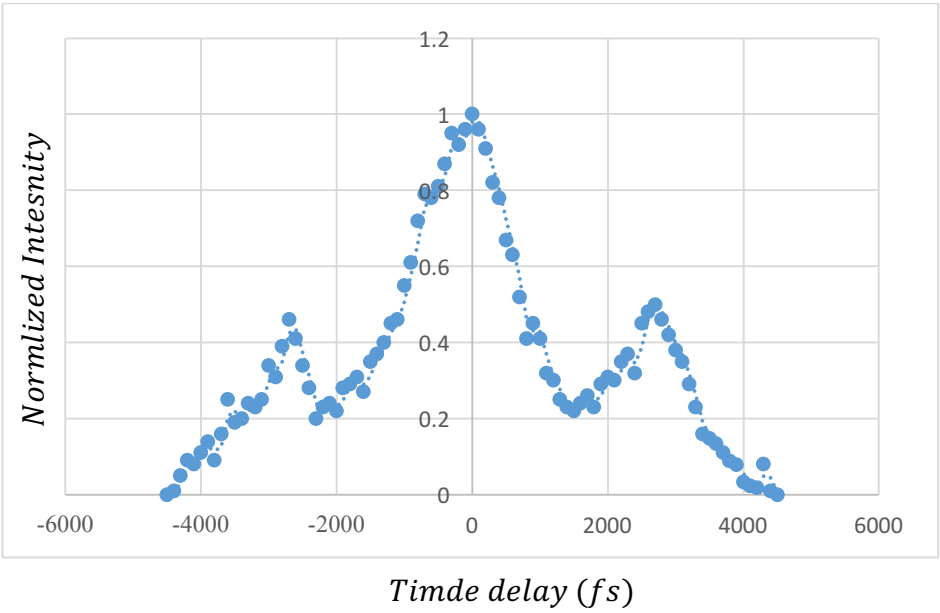

Figure 4.20: Experimental Autocorrelation curve of first anti-Stokes order in the presence of red-shifted shoulder

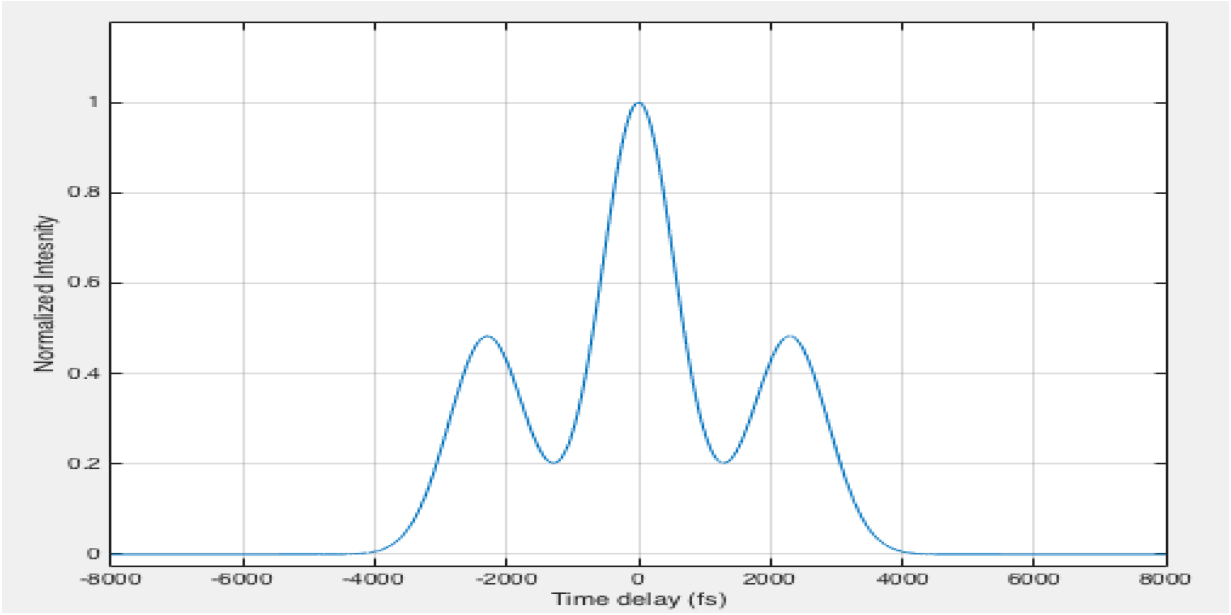

Figure 4.21: Simulated Autocorrelation curve of first anti-Stokes order in the presence of red-shifted shoulder

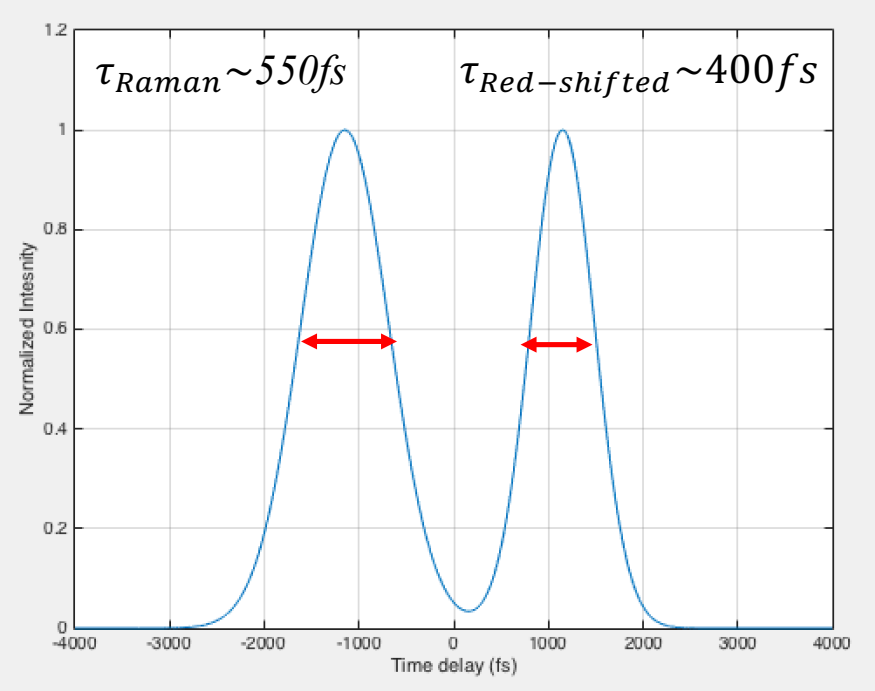

Figure 4.22: The two Gaussian pulses input, which will construct the 4.21 curve

Figure 4.20 shows the experimental result of the compressed pulse. We used the Gaussian pulses in figure 4.22 to construct the experimental result, which is presented in figure 4.21.

Our experimental autocorrelation curves show that the separation between the peaks is around 2.3ps. The duration of the Raman pulse is around 550 fs, and the duration of the red-shifting pulse is around 400fs.

Prims separation: 3.5 m

Duration of Raman Pulse: 550 fs

Duration of red-shifting pulse: 400 fs

Temporal delay between the pulses: 2300 fs

Third Autocorrelation Curve and Pulse Reconstruction: (Prism separation ~3m)

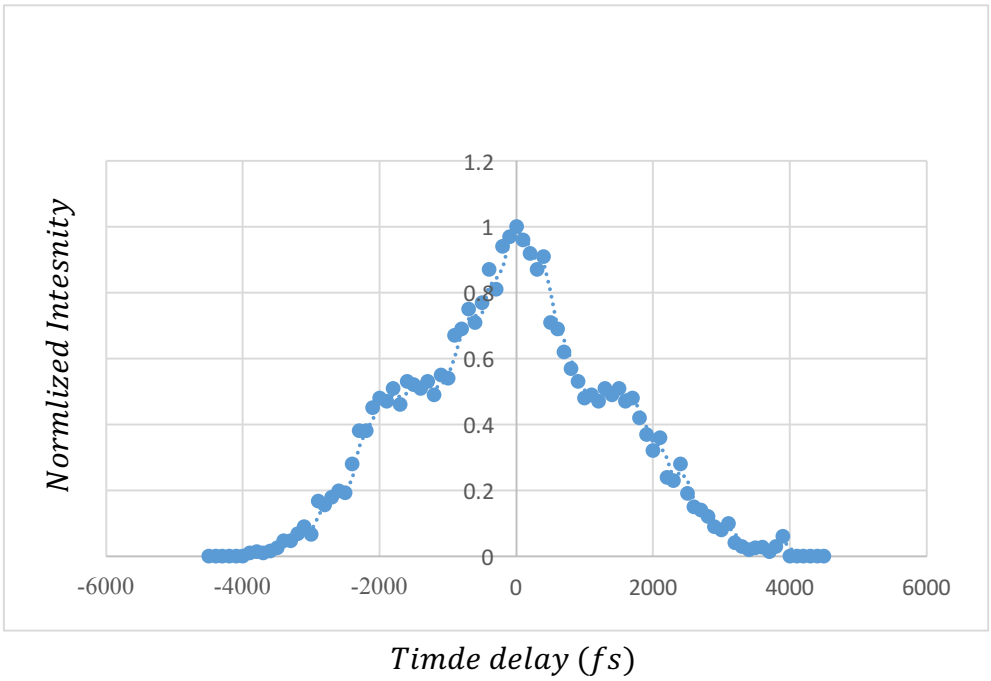

Figure 4.23: Experimental Autocorrelation curve of first anti-Stokes order in the presence of red-shifted shoulder

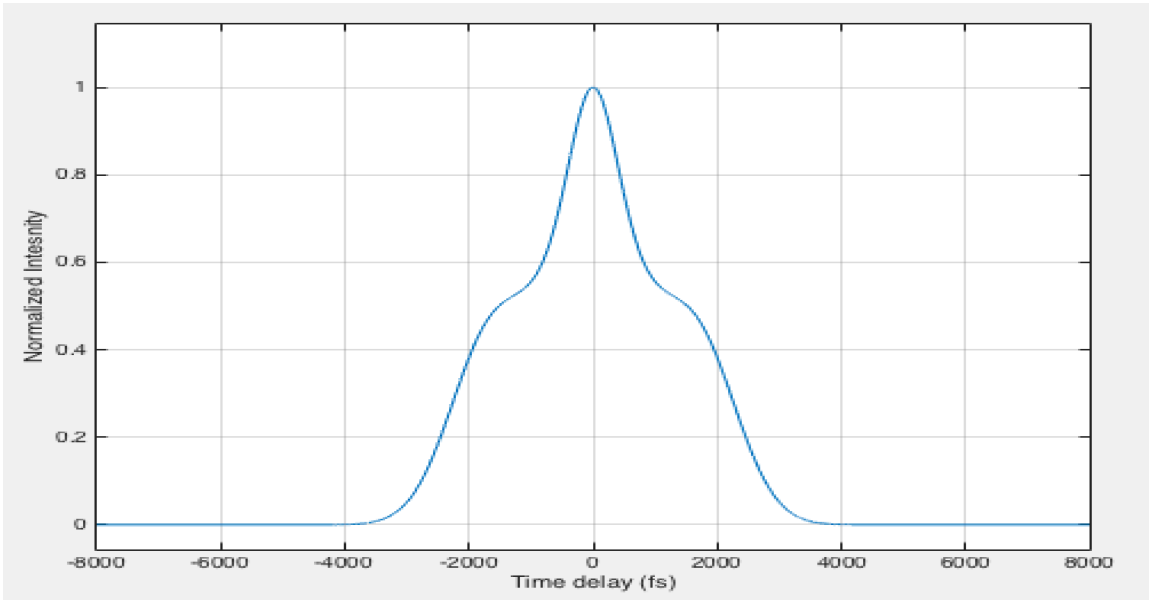

Figure 4.24: Simulated Autocorrelation curve of first anti-Stokes order in the presence of red-shifted shoulder

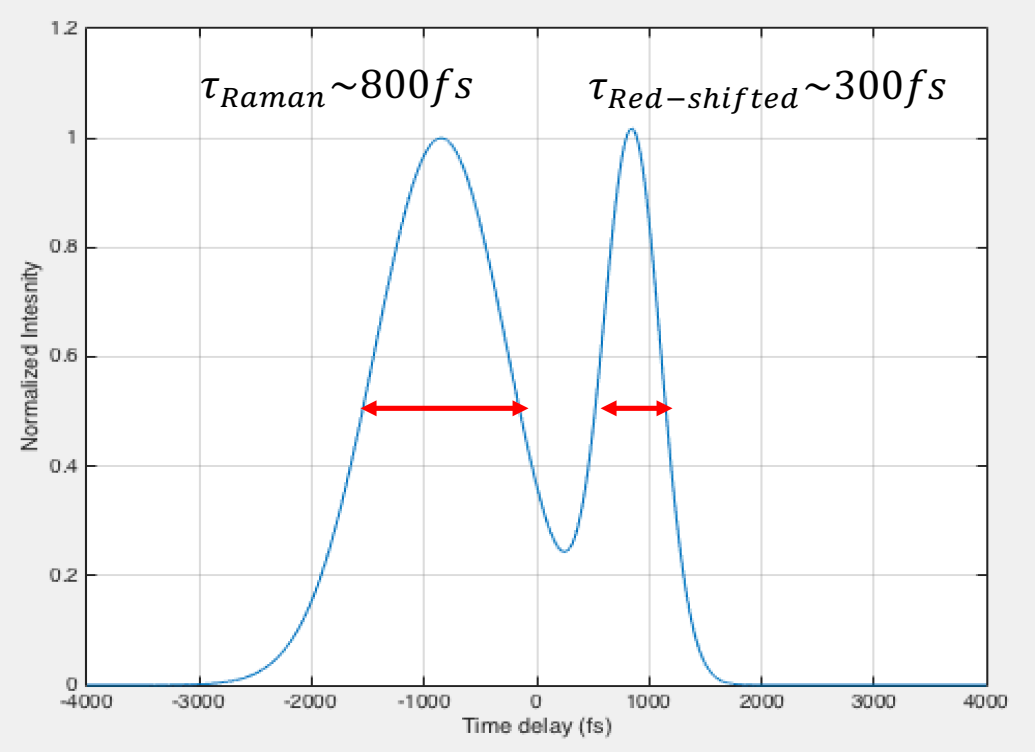

Figure 4.25: The two Gaussian pulses input, which will construct the 4.24 curve

Figure 4.23 shows the experimental result of the compressed pulse. We used the Gaussian pulses in figure 4.25 to construct the experimental result, which is presented in figure 4.23.

Our experimental autocorrelation curves show that the separation between the peaks is around 1.7ps. The duration of the Raman pulse is around 800 fs, and the duration of the red-shifting pulse is around 300 fs.

Prims separation: 3 m

Duration of Raman Pulse: 800 fs

Duration of red-shifting pulse: 300 fs

Temporal delay between the pulses: 1700 fs

4.3 Discussion

As we have shown in the last section, we can use our pulse compression system to compress the first Raman anti-Stokes order in the presence and absence of red-shifted shoulder. We have seen that in the presence of red-shifted shoulder, our autocorrelation curve shows three separate peaks. These peaks means that we have two different pulses with a temporal delay between them.
Because of this delay, our optical pulse compression system cannot combine and compress these two pulses together.
We have seen that by changing the separation between the prisms in our pulse compressor, the duration of the reconstructed pulses will be changed. Table 4.1 shows the duration of the Raman and the red-shifted pulse for different prisms separations.

Prisms separation	Duration of Raman pulse	Duration Red-shifted pulse
3m	800fs	300fs
3.5m	550fs	400fs
4m	380fs	500fs

Table 4.1: Duration of reconstructed Raman pulse and Red-shifted pulse for different prisms separations

The first conclusion from table 4.1 is that the Raman pulse and the red-shifted pulse has different spectral phase behavior. Our pulse compression setup is designed to compress different Raman orders. These Raman orders will have approximately the same chirp rate as the pumps have. As we can see from table 4.1, by changing the prism separation from 3m to 4m, the Raman pulse is going to be compressed from 800fs to 380 fs, but the red-shifted pulse is going to be broadened from 300 fs to 500 fs. This means that they do not have the same spectral phase. By using equation 2.17, we can calculate that how much dispersion our compressor will provides for different prims separations. If the separation between the prisms be 3m the GDD of the pulse compressor will be $-10{,}000fs^2$, if the separation be 3.5m the GDD of the compressor will be $-40{,}000fs^2$, and finally if the separation between the prims be 4m the GDD will be around $-80{,}000fs^2$. Table 4.2 shows the calculated amount of dispersion for different prims separation.

Prisms separation	Group delay dispersion (GDD)
3m	≈ -10,000 fs^2
3.5m	≈ -40,000 fs^2
4m	≈ -80,000 fs^2

Table 4.2: GDD of the prisms compressor as a function of prisms separation

By using equation 2.29, the duration of transform limited red-shifted pulse will be around 270fs. Now we can use the results of table 4.2 to calculate the duration of Red-shifted pulse for different prisms separations.

Prisms separation	Duration of red-shifted pulse
3m	≈ 300 fs
3.5m	≈ 490 fs
4m	≈ 850 fs

Table 4.3 Calculated duration of red-shifted pulse as a function of prisms separation

Table 4.3 shows the calculated duration of the red-shifted pulse if we add a known amount of dispersion to the transform limited limited red-shifted pulse. Table 4.1 shows that the measured duration of red-shifted pulse by using the autocorrelation curves. Both of these tables confirms that the duration of the red-shifted pulse will be increased by adding more dispersion. This means that the red-shifted pulse does not have the same phase behavior like the Raman pulse.

Our data also shows that the temporal delay between the pulses will be changed for different prims separations. This is a rational result and coming from the fact that the two pulses will have different optical paths inside the compressor, and when we change the prism separation the temporal delay between the pulses will be changed because the difference between the optical paths will be changed too. Table 4.2 shows temporal delay between the pulses as function of prims separation.

Prism separation	Temporal delay
3m	1700 fs
3.5m	2300 fs
4m	2600 fs

Table 4.4: Temporal delay between the pulses as a function of prism separation

Figure 4.26 shows that two beams with different wavelength will have different optical paths inside the prism compressor. We can calculate the difference between these optical paths, then we can approximately say that how much was the temporal delay between the pulses before entering the prims compressor. Our calculation shows that if the separation between the prims be 4m, the compressor will cause 1.1 ps delay. This means that the temporal delay between the pulses will be around 1.5 ps before entering the compressor.

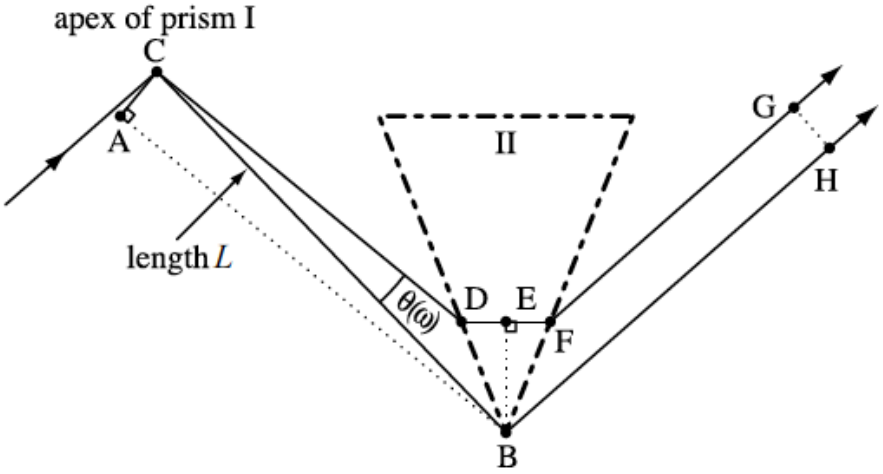

Figure 4.26: Illustration of different optical paths of two beams inside a prims pair compressor [26]

Conclusion and Future Work

The primary goal of this research was to study the effect of the red-shifting process in MRG. We have seen that by pumping the SF_6 in the transient regime, the Raman orders will have the red-shifted shoulder, which even doubles the frequency bandwidth of each Raman order. This red-shifting process can be useful to increase ultimate peak power of each pulse.

In this thesis, we used a prism pair setup to compress the Raman order in the absence and presence of red-shifted shoulder. We have shown that in the absence of red-shifted shoulder it is possible for us to compress the first anti-Stokes order close to its Fourier transform limit. In the presence of a red-shifted shoulder, we have seen that the first anti-Stokes order contains two separate pulses. Our results show that there is a temporal delay between the two pulses. We have used our prism pair to study this delay, and we have seen by changing the separation between the prisms the delay between the pulses will be changed. This change in the delay confirms that these two pulses are independent of each other. We have also seen that the by changing the prism separation the temporal duration of the pulses will change differently, or in the other word if we want to compress the Raman pulse, the red-shifting pulse will be broadened. This shows that they do not have the same spectral phase, which is very interesting for us.

The next step in our research is to apply this compression technique to other Raman orders. Then we are planning to use an Acousto-optic programmable dispersive filter to combine different Raman orders and try to add them coherently to get short lasers pulses with the duration of one femtosecond.

References

[1] G. 9:13, Bible.

[2] R. Ell, U. Morgner, F. Kartner, J. Fujimoto, E. Ippen, V. Scheuer, G. Angelow, T. Tschudi, M. Lederer, A. Boiko and B. Luther-Davies, "Generation of 5-fs pulses and octave-spanning spectra directly from a Ti:sapphire laser," Optics Letter, Vol. 26, Issue 6, pp. 373-375 (2001).

[3] K. Midorikawa, " High-Order Harmonic Generation and Attosecond Science" Japanese Journal of Applied Physics 50 , Vol. 50, Number 9R, 2011.

[4] F. McClung and R. Hellwarth, "Giant Optical Pulsations from Ruby," Applied Optics, Vol. 1, Issue S1, pp. 103-105, 1962.

[5] A. Yariv and P. Yeh, "Optical waves in crystals," Wiley-Interscience Publications, 1984.

[6] U. Keller, D. Miller , G. Boyd , T. Chiu, J. Fergosun and M. Asom, "Solid-state low-loss intracavity saturable absorber for Nd:YLF lasers: an antiresonant semiconductor Fabry–Perot saturable absorber," Optics Letter, Vol. 17, Issue 7, pp. 505-507 ,1992.

[7] U. Keller, "Ultrafast solid-state laser oscillators: a success story for the last 20 years with no end in sight," Appl Phys B, Vol. 100, Issue 1, pp 15–28, 2010.

[8] D. Spence, P. Kean and W. Sibbet, "60-fsec pulse generation from a self-mode-locked Ti:sapphire laser," Optics Letter, Vol. 16, Issue 1, pp. 42-44, 1991.

[9] S. Chen and J. Wang , "Self-starting issues of passive self-focusing mode locking," Optics Letters, Vol. 16, Issue 21, pp. 1689-1691, 1991.

[10] T. Gaumnitz, A. Jain, Y. Pertot, M. Huppert, F. Ardana-Lamas and H. Wörner, "Streaking of 43-attosecond soft-X-ray pulses generated by a passively CEPstable," Optics Express, Vol. 25, Issue 22, pp. 27506-27518, 2017.

[11] S. Baker, I. Walmsley, J. Tisch and J. Marangos, "Femtosecond to attosecond light pulses from a molecular modulator," Nature Photonics 5, pages 664–671, 2011.

[12] F. Pandarese and C. Townes, "Coherently Driven Molecular Vibrations and Light Modulation," Physics Review Letter, Vol. 11, NUMBER 4 , 1963.

[13] H. Chan, Z. Hsieh, W. Liang, A. Kung and C. Lee, "Synthesis and measurement of ultrafast waveforms from five discrete optical," Science, Vol. 331, Issue 6021, pp. 1165-1168 ,2011.

[14] A. H. Zewail, "F. Laser Control and Femtosecond Dynamics. Femtosecond Dynamics of Reactions: Elementary Processes of Controlled Solvation," 1995.

[15] S. Harris and A. Sokolov, "Broadband spectral generation with refractive index control," PHYSICAL REVIEW A, Vol. 55, NUMBER 6, 1996.

[16] M. Katsuragawa, K. Yokoyama, T. Onose and K. Misawa, "Generation of a 10.6-THz ultrahigh-repetition-rate train by synthesizing phase-coherent Raman-sidebands," Optics Express, Vol. 13, Issue 15, pp. 5628-5634, 2005.

[17] Belenov E. M., Nazarkin A. V., Prokopovich I. P, "Dynamics of an intense femtosecond pulse in a Raman-active medium," Pisma ZhETF, Vol. 55, ISSUE 4 , PAGE 218, 1992.

[18] J.-K. Wang, Y. Siegal, C. Lü, E. Mazur and J. Reintjes, "Subpicosecond stimulated Raman scattering in highpressure," Journal of the Optical Society of America B, Vol. 11, Issue 6, pp. 1031-1037 , 1994.

[19] V. Krylov, O. Ollikainen, U. Wild, A. Rebane, V. Bespalov and D. Staselko, "Femtosecond stimulated Raman scattering in pressurized gases in the

ultraviolet and visible spectral ranges," Journal of the Optical Society of America B, Vol. 15, Issue 12, pp. 2910-2916, 1998.

[20] A. Nazarkin, G. Korn, M. Wittmann and T. Elsaesser, "Generation of Multiple Phase-Locked Stokes and Anti-Stokes Components in an Impulsively Excited Raman Medium," Phys. Rev. Lett, Vol. 83, Number 13, 1999.

[21] A. Nazarkin, G. Korn and T. Elsaesser, "All-linear control of attosecond pulse generation", Vol. 203, Issues 3–6, pp. 403-412, 2002.

[22] V. Kalosha and J. Herrmann, "Pulse compression without chirp control and frequency detuning by high-order coherent Raman scattering in impulsively excited media," Optics Letters, Vol. 26, Issue 7, pp. 456-458, 2001.

[23] V.Kalosha, M.Spanner, J.Herrmann, and M. Ivanov, "Generation of single dispersion precompensated 1-fs pulses by shaped-pulse optimized high-order stimulated Raman scattering", Phys Rev Lett, Vol. 88, Number 10, 2002.

[24] N. Zhavoronkov and G. Korn, "Generation of Single Intense Short Optical Pulses by Ultrafast Molecular Phase Modulation," Phys. Rev. Lett, Vol. 88, Number 20, 2002.

[25] F. Noack, O. Steinkellner, P. Tzankov, H. Ritze and Y. Kida, "Generation of sub-30 fs ultraviolet pulses by Raman induced phase modulation in nitrogen," Optics Express, Vol. 13, Issue 7, pp. 2467-2474, 2005.

[26] V. P. Kalosha and J. Herrmann, " Ultrawide spectral broadening and compression of single extremely short pulses in the visible, uv-vuv, and middle infrared by high-order stimulated Raman scattering," Physical Review, 2003.

[27] Y. Irie and T. Imasaka, "Generation of vibrational and rotational emissions by four-wave Raman mixing using an ultraviolet femtosecond pump beam," Optics Letters, Vol. 20, Issue 20, pp. 2072-2074, 1995.

[28] E. Sali, K. Mendham, J. Tisch, T. Halfmann and J. Marangos, "High-order stimulated Raman scattering in a highly transient regime driven by a pair of ultrashort pulses," Optics Letters, Vol. 29, Issue 5, pp. 495-497, 2004.

[29] A. Sokolov, D. Walker, D. Yavuz, G. Yin and S. Harris, "Femtosecond Light Source for Phase-Controlled Multiphoton Ionization," Physical Review Letters, Vol. 87, Number 3, 2001.

[30] D. Strickland, Z. Cui, M. Chaturvedi and H. Yan, "Multi-frequency Raman Generation with Chirped Pumping," JSAP-OSA Joint Symposia 2013 Abstracts, paper 18p_D5_1, 2013.

[31] J. C. White, Tunable Lasers, Springer, 1987.

[32] Z. Cui, M. Chaturvedi, B. Tian, J. Ackert, F. Turner and D. Strickland, "Spectral red-shifting of multi-frequency Raman orders," Optics Communications, Vol 288, pp. 118-121 , 2013.

[33] "Refractive index database," [Online]. Available: https://refractiveindex.info/?shelf=glass&book=BAF10&page=SCHOTT.

[34] F. Jenkins and H. White, Fundamentals of Optics, McGraw-Hill, 1957.

[35] A. Weiner, Ultrafast Optics, John Wiley & Sons, Inc, October 2008.

[36] E. Treacy, "Optical pulse compression with diffraction gratings," IEEE Journal of Quantum Electronics, Vol. 5, no. 9, pp. 454 - 458,1969.

[37] O. Martinez, J. Gordon and R. Fork, "Negative group-velocity dispersion using refraction," Journal of the Optical Society of America A, Vol. 1, Issue 10, pp. 1003-1006, 1984.

[38] C. Froehly, B. Colombeau and M. Vampouille, "Shaping and Analysis of Picosecond Light Pulses," Progress in Optics, Vol. 20, pp. Pages 63-153, 1983.

[39] R. Fork, O. Martinez and J. Gordon, "Negative dispersion using pairs of prisms," Optics Letters, Vol. 9, Issue 5, pp. 150-152, 1984.

[40] R. Trebino. [Online]. Available: http://frog.gatech.edu/talks.html.

[41] R. Trebino, Frequency-Resolved Optical Gating: The Measurement of Ultrashort Laser Pulses, SPRINGER , 2000.

[42] Z. Zhang, A. Deslauriers and D. Strickland, "Dual-wavelength chirped-pulse amplification system," Optics Letters, Vol. 25, Issue 8, pp. 581-583, 2000.

[43] M. Lai, S. Lai and C. Swinger, "Single-grating laser pulse stretcher and compressor," Applied Optics, Vol. 33, Issue 30, pp. 6985-6987, 1994.

[44] W. Niblack and E. Wolf, "Polarization Modulation and Demodulation of Light," Applied Optics, Vol. 3, Issue 2, pp. 277-279, 1964.

[45] L. Frantz and J. Nodvik, "Theory of Pulse Propagation in a Laser Amplifier," Journal of Applied Physics, Vol. 34, Issue 8, 1963.

[46] H. Yan, "Characterizing Transient Regime Multi-frequency Raman Generation by the Aid of Spectral Phase Interferometry for Direct Electric-field Reconstruction," Waterloo, 2013.

[47] A. Yariv and P. Yeh, Optical waves in crystals, NewYork: John Wiley & Sons, Inc, 1984.

[48] P. Russell, "Photonic Crystal Fibers," science, Vol. 299, Issue 5605, pp. 358-362, 2003.

[49] F. Benabid , J. Knight, G. Antonopoulos and P. Russell, "Stimulated Raman scattering in hydrogen-filled hollow-core photonic crystal fiber.," Science, Vol. 298, Issue 5592, pp. 399-402, 2002.

[50] F. Salin, P. Georges, G. Roger and A. Brun, "Single-shot measurement of a 52-fs pulse," Applied Optics, Vol. 26, Issue 21, pp. 4528-4531, 1987.